Journal of Materials Chemistry C

ROYAL SOCIETY OF CHEMISTRY

REVIEW

View Article Online
View Journal | View Issue

Cite this: J. Mater. Chem. C, 2021, 9, 13041

Modern aspects of strategies for developing single-phase broadly tunable white light-emitting phosphors

Sayed Ali Khan,[ab] Noor Zamin Khan,[c] Muhammad Sohail,[d] Jahangeer Ahmed,[e] Norah Alhokbany,[e] Saad M. Alshehri,[e] Xin Xu,[c] Jinfeng Zhu *[ab] and Simeon Agathopoulos[f]

In phosphors intended for the applications of white light-emitting diodes (white-LEDs), their ability to achieve controlled-photoluminescence-tuning is an important feature, which is directly linked to their optimization and modification. More specifically, the development of luminescent materials with broadly and continuously tunable photoluminescence is still a challenge for the generation of highly efficient warm white-light with appropriate correlated color temperature (CCT), a high color-rendering-index (CRI), and excellent thermal stability. This review presents the latest developments of single-phase white-light-emitting $Ba_9Lu_2Si_6O_{24}$ (BLSO) silicate phosphors. The emerging approaches to crystal-site engineering and the energy transfer mechanisms are discussed at great length. The BLSO phosphor host lattice, having rich and distinguishing crystallographic sites, provides various surrounding environments to the doped rare-earth (RE) ions, and it also allows for the engineering of the local atmosphere of the doped ions. Substitution with more than one activator, as a co-dopant ion, in the BLSO phosphor host may enable tuning of the photoluminescence spectrum to the desired spectral region. The ultimate goal of this review is to aid research aimed at discovering new approaches to the aforementioned objectives, following strategies associated with the occupation of multiple crystallographic sites with activators, in accordance with a thorough understanding of the function of the energy-transfer phenomenon, whereby various dopants can achieve efficient tunability.

Received 24th June 2021,
Accepted 20th August 2021

DOI: 10.1039/d1tc02952e

rsc.li/materials-c

1. Introduction

About 20% of the electricity produced globally is consumed to cover the needs for lighting. Thus, more efficient sources of illumination will save an enormous amount of energy. Nonetheless, the production of efficient white light, which would be a promising solution for indoor illumination, still remains a great challenge. In order to obtain a high-quality color in an accurate way, the source of illumination needs to provide photons at visible-spectrum wavelengths. The achievement of such a broadband emission from single-phase phosphors is an exciting challenge.

In commercially available white-light sources, one or more light-emitting diodes (LEDs), coated with one or more phosphors, yield a combined emission that appears to be white. Nevertheless, multiple emitters result in a variation of emission color over time, due to the unequal rates of degradation of the emitters, and in a loss of efficiency, owing to reabsorption, which leads to overlapping of the absorption and emission energies of the various components.[1–4] An ideal solution would be a single material that emits broadband white light with a continuous emission spectrum (400–700 nm).[5–8]

The host lattice of phosphor compositions, which have multiple crystallographic sites, provides the opportunity of tuning the luminescence within the entire visible spectrum by manipulating the surrounding environment around the doped

[a] School of Electronic Science and Engineering, Fujian Provincial Key Laboratory of Electromagnetic Wave Science and Detection Technology, Xiamen University, Xiamen 361005, P. R. China. E-mail: nanoantenna@hotmail.com
[b] State Key Laboratory of Applied Optics, Changchun Institute of Optics, Fine Mechanics and Physics, Chinese Academy of Sciences, Changchun 130033, China
[c] CAS Key Laboratory of Materials for Energy Conversion, School of Chemistry and Materials Science, University of Science and Technology of China, Hefei, Anhui 230026, P. R. China
[d] International Collaborative Laboratory of 2D Materials for Optoelectronics Science and Technology, Engineering Technology Research Center for 2D Material Information Function Devices and Systems of Guangdong Province, Shenzhen University, Shenzhen 518060, China
[e] Department of Chemistry, Collage of Science, King Saud University, P.O. Box 2455, Riyadh 11451, Saudi Arabia
[f] Department of Materials Science and Engineering, University of Ioannina, GR-451 10 Ioannina, Greece

activators. Because of the mismatch between the activator and the host cation at a particular crystallographic site, the activator may occupy the most suitable site.[9–11] More specifically, a broad 5d–4f transition is usually observed in divalent Eu^{2+}, Sm^{2+}, and Yb^{2+}, and trivalent Ce^{3+} rare-earth ions.[12–14] The $4f^n$ ground state is completely shielded by the surrounding 5s and 5p orbitals. The 5d level of the $5d^{n-1}$–$4f^1$ excited state is not fully shielded, and therefore, it is more sensitive to the surrounding environment of the host lattice. This phenomenon causes a shift of the emission and excitation spectra up to several tenths of nanometers,[15,16] while the positions of excitation and emission remain almost the same in the case of $4f^n$ transition. Accordingly, the position of the 5d level, which shifts depending on the host composition, is responsible for changes in the difference in energy between the ground and excited levels.

Furthermore, various factors, like crystal-field splitting and the nephelauxetic effect, also influence photoluminescence excitation and emission tuning.[14,17] Divalent Eu^{2+} ions mostly exhibit orange and red emission in nitrides, while UV and blue emission is exhibited by fluorides.[18–20] The 4f–4f transition in most of the trivalent lanthanides results in its characteristic emission lines, whose peak positions remain almost fixed or they slightly shift on account of the changes in the phosphor host lattice due to the forbidden 4f–4f transition,[21–23] whereas the 5d level of the spin-allowed transition of Ce^{3+}/Eu^{2+} is highly sensitive to the surrounding environment of the host lattice, such as the centroid shift and crystal-field splitting.[24–26] The centroid shift is linked to the polarizability of the surrounding anion ligands and to the covalency of the crystal.[27,28] The extent of crystal-field splitting depends on the bond lengths between the activator ion and the coordinating anions, the degree of covalency between the activator ion and its ligands, the coordination environment, and the symmetry of the site of the activator.[29,30] The fundamental understanding of the relationship between the luminescence of phosphors and the host lattice still poses an interesting challenge.

A. Kalaji[31] and co-workers investigated the photoluminescence excitation and emission spectra along with the behavior of thermal quenching and thermal degradation of phosphors, which can be tuned through variation of phosphor-host composition and structure. They substituted the tetravalent Si^{4+} with Al^{3+} and Ge^{4+} in the gamma-phase Ca_2SiO_4-phosphor host lattice. This caused a redistribution of the doped Ce^{3+} in two distorted available crystallographic sites of Ca^{2+}. As a result, the high-energy blue emission was efficiently shifted to yellow emission. The double substitution of Mg^{2+} and Si^{4+}/Ge^{4+} caused an appropriate redshift in the emission spectrum of YAG:Ce^{3+} garnet phosphors under blue-light irradiation.[32]

Our previous work investigated the occupation of divalent Eu^{2+} ions in the three distinct crystallographic sites of Ba^{2+} in $Ba_9Lu_2Si_6O_{24}$ silicate phosphors.[33] When the concentration of Eu^{2+} was low ($x < 0.1$), the Eu^{2+}-doped $Ba_9Lu_2Si_6O_{24}$ phosphors generated efficient blue light with a dominating peak at around 462 nm. However, as the Eu^{2+} concentration was increased ($x > 0.3$), both the photoluminescence excitation and emission were efficiently tuned (PLE from 342 to 452 nm, and PL from 462 to 512 nm). The efficient tuning of the photoluminescence excitation enables a perfect matching of the green emission of the synthesized phosphors with the blue emission of an InGaN

Sayed Ali Khan

Dr Sayed Ali Khan was born in Swabi, KPK Pakistan. He received his Master's degree in Physics (2014) from Abdul Wali Khan University Mardan, Pakistan. He received his PhD in Materials Science and Engineering (2017) from the University of Science and Technology of China under the supervision of Professor Xin Xu. From January 2018 to December 2019, he was a Postdoctoral Fellow in the Department of Microscale Optoelectronics, Shenzhen University. To date, he has been with Xiamen University, Xiamen, Fujian, China, involved in research on luminescent materials for white LEDs. Recently, he was selected as a visiting scholar at Rutgers University, USA. He has published 54 papers and 1 book chapter in an international peer-reviewed journal as an author and a coauthor. His current research focuses on the development of broadly tunable luminescent materials for white LEDs and displays.

Jinfeng Zhu

Prof. Jinfeng Zhu received his BS degree in electronic communication science and technology and his PhD degree in physical electronics from the University of Electronic Science and Technology of China, Chengdu, Sichuan, China, in 2006 and 2012, respectively. From November 2009 to November 2011, he was a visiting PhD student in the Department of Electrical Engineering, University of California, Los Angeles, CA, USA. From July 2017 to July 2018, he was a visiting professor in the Optoelectronics Research Centre, University of Southampton, Hampshire, UK. Since July 2012, he has been with Xiamen University, Xiamen, Fujian, China, where he is currently the Associate Dean and Professor in the Institute of Electromagnetics and Acoustics. He has authored and coauthored more than 60 peer reviewed journal papers. His research interests include nanoantennas, nanophotonics, plasmonics, metamaterials, van der Waals materials, and related sensing applications. He is a Senior Member of the IEEE and serves as the Topic Editor of Sensors and Associate Editor of Frontiers in Materials.

chip. This qualifies them for possible application in multicolor white LEDs (RGB LEDs).

Besides adding to the cost of the final product, a further increase of Eu concentration may also result in concentration quenching, which decreases the photoluminescence intensity. Cation-size mismatch, neighboring-cation substitution, and release of neighboring cation-induced stress have been proposed in order to tune photoluminescence and thermal quenching.[34–37] To avoid concentration quenching, efficient substitution with Sr^{2+} and Ca^{2+} cations, with comparably smaller ionic radii, in $Ba_9Lu_2Si_6O_{24}$ was attempted at a low concentration of Eu^{2+} (x = 0.1).[33,38] The former substitution caused a shift of photoluminescence emission to a longer wavelength, having a maximum at 512 nm, owing to the doping Eu^{2+} activators occupying the Ba(3) crystallographic site, which has a different coordination environment than that in the Ba(1) site, having blue emission at 462 nm. The latter substitution showed a broadband emission spectrum that covers the blue (430–480 nm), green (500–550 nm), and yellow (560–580 nm) spectral regions, on account of the distribution of the doping Eu^{2+} activators among the three crystallographic sites, which have different surrounding environments. The luminescence characteristics of various dopants in $Ba_9Ln_2Si_6O_{24}$ (Ln = Sc^{3+}, Y^{3+}, Lu^{3+}, and Al^{3+}) orthosilicate phosphors are summarized in Table 1.

The emission of the various color components in the visible spectral region can be generated by the single-phosphor host lattice by co-doping with various sensitizers and activators with the mechanism of multiple energy transfer (ET), leading to attractive multicolor emission.[51,52] Consequently, the development of phosphors with various emission colors due to their ET characteristics becomes a key issue for single-phase phosphor-converted white LEDs.

As discussed above, the phosphor composition, having multiple crystallographic sites, offers the versatility of sites for occupation with various sensitizer and activator ions. As a result, the photoluminescence excitation (PLE) and emission (PL) may be easily tuned to the appropriate spectral range. Additionally, this can also increase the photoluminescence quantum yields (PLQYs) of coactivated transition metal and rare-earth ions, whose d–d and f–f transitions are parity forbidden due to ET from the sensitizer, which has a 5d–4f parity allowed transition. In this case, the ET mechanism determines the generation of light with longer wavelengths (green, yellow, and red). More specifically, the sensitizer Ce^{3+}/Eu^{2+}, having a 5d–4f parity allowed transition, absorbs UV, NUV, and blue light, and emits at shorter wavelengths of the visible spectrum. This low-wavelength emission (blue to cyan) is absorbed by the other (co-doped) activators, resulting in an emission at a longer wavelength (green, yellow, or red).

The combination of the emissions generated by various activators can be adjusted to the resultant white light. The adjustment of the emission depends on the activators and the appropriate host–ligand field.[53–55] Various transition-metal and rare-earth ions, such as Bi^{3+}, Eu^{2+}, Ce^{3+}, Tb^{3+}, Dy^{3+}, and Sm^{3+}, are efficient sensitizers, which effectively transfer part of their energy to various activators, like Tb^{3+}, Eu^{3+}, Mn^{2+}, Mn^{4+}, Sm^{3+}, Dy^{3+}, and Eu^{2+} ions. Tuning of photoluminescence emission has been enabled due to the ion–ion interactions of various sensitizer/activator couples, such as Eu^{2+}/Mn^{2+},[56] Eu^{2+}/Tb^{3+},[57,58] and Ce^{3+}/Tb^{3+},[59] in the lattice of many phosphor hosts. Our previous studies report on examples of the ion–ion interactions of various couples in single-phase phosphors, like $CaLa_4Si_3O_{13}$:Ce^{3+}/Tb^{3+},[55] $Y_5Si_3O_{12}N$:Ce^{3+}/Tb^{3+},[60] $Ca_xBa_{9-x}Lu_2Si_6O_{24}$:$Eu^{2+}$/$Mn^{2+}$,[38] $Ba_9Lu_2Si_6O_{24}$:Ce^{3+}/Tb^{3+}/Mn^{2+},[61] YPO_4:Dy^{3+}/Eu^{3+}/Tb^{3+},[62] Ca_2YTaO_6:Bi^{3+}/Eu^{3+},[63] Ca_2LuTaO_6:Dy^{3+}/Eu^{3+},[64] and $Y_5Si_3O_{12}N$:Ce^{3+}/Dy^{3+}.[65] The tunable photoluminescence emission of such ion–ion interactions enriches the family of phosphor-converted white LEDs and meets the requirements of multiple applications and various advanced optical devices.

This review thoroughly reports on the latest developments as far as the emerging aspects of designing novel compositions of single-phase white light-emitting phosphors are concerned. More specifically, we selected the phosphor host lattice of $Ba_9Lu_2Si_6O_{24}$, as a model, because it has multiple crystallographic sites for occupation with various activators; it generalizes all lattices of phosphor-hosts that have multiple crystallographic sites. We provide a comprehensive study of the tuning of photoluminescence emission owing to the occupation of multiple crystallographic sites of single-phase phosphors with activators. Effective control of the tuning of the emission color as a result of the efficient energy transfer in double- and triple-doped single-phase phosphor hosts is also a focal point in this study.

Table 1 Luminescence features of various dopants in $Ba_9Ln_2Si_6O_{24}$ (Ln = Sc^{3+}, Y^{3+}, Lu^{3+}, and Al^{3+}) orthosilicate phosphors

Composition	λ_{ex} (nm)	λ_{em} (nm)	Energy transfer	Ref.
$Ba_9Sc_2Si_6O_{24}$:Ce^{3+}	325	384	—	39
$Ba_9Sc_2Si_6O_{24}$:Eu^{2+}	450	508	—	40
$Ba_9Y_2Si_6O_{24}$:Ce^{3+}	394	480	—	41
$Ba_9Y_2Si_6O_{24}$:Eu^{2+}	420	506	—	42
$Ba_9Y_2Si_6O_{24}$:Bi^{3+}/Eu^{3+}	337, 372	408, 501	Yes	43
$Ba_9Y_2Si_6O_{24}$:Sm^{3+}	404	603	—	44
$Ba_9Al_2Si_6O_{24}$:Ce^{3+}	328	386	—	45
$Ba_9Al_2Si_6O_{24}$:Eu^{2+}	—	—	—	
$Ba_9Lu_2Si_6O_{24}$:Ce^{3+}	400	490	—	46
$Ba_9Lu_2Si_6O_{24}$:Eu^{2+}	342	460	Yes	47
$Ba_9Lu_2Si_6O_{24}$:Eu^{2+}	440	514	—	48
$Ba_9Lu_2Si_6O_{24}$:Bi^{3+}/Eu^{3+}	335, 370	410, 485	Yes	49
$Ba_9Lu_2Si_6O_{24}$:Tb^{3+}	251	552	—	50

2. Crystal structure of the BLSO phosphor host lattice

BLSO crystallizes in the rhombohedral system with space group $R3$ and has three distinct crystallographic sites. More specifically, the rhombohedral structure of BLSO (Fig. 1a) consists of corner-sharing SiO_4–LuO_6–SiO_4 layers, creating a 3D framework. The Lu^{3+} ions form a twisted LuO_6 octahedron with three short (2.160 Å) and three long (2.223 Å) Lu–O bonds, which are coordinated by six oxygens. The 12-coordinated Ba(1), the

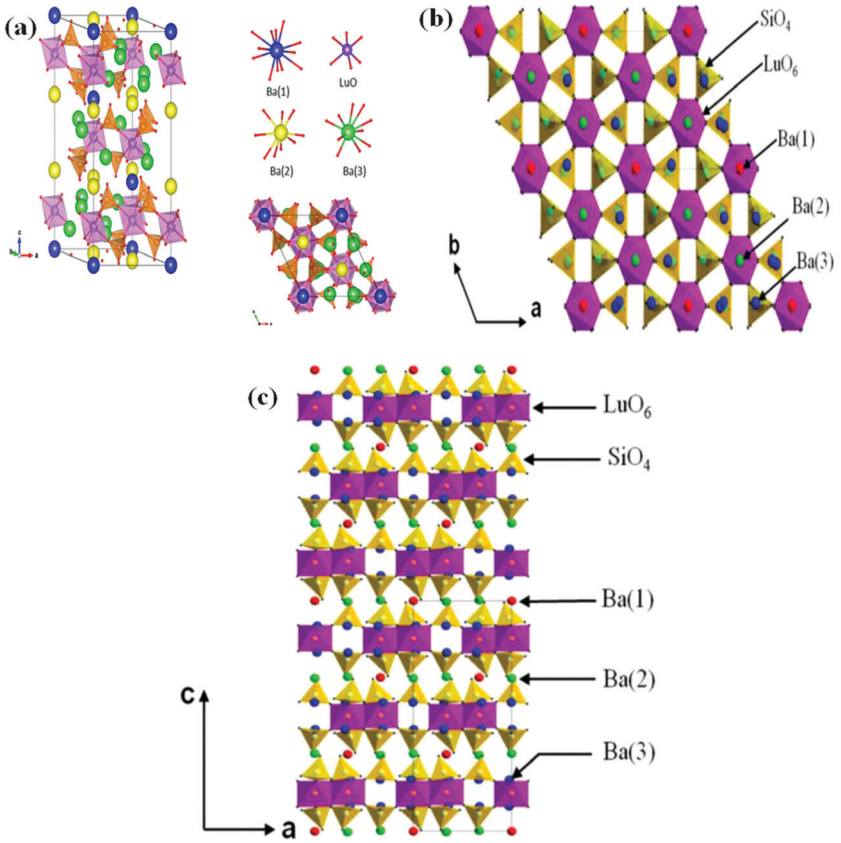

Fig. 1 Various features, such as the crystal structure (a) viewed perpendicularly to the *b* and *c* axes with the coordinated environment of Ba(1), Ba(2), Ba(3), and Lu with oxygen, with magnified structures (b) perpendicular to the *c* axis, and (c) perpendicular to the *b* axis.[66,90] (Reproduced with permission from ref. 90, copyright 2016, American Chemical Society and ref. 66, copyright 2015 Wiley.)

9-coordinated Ba(2), and the 10-coordinated Ba(3) have three different sites for oxygen, with average Ba–O bond lengths as 3.085, 2.925, and 2.934 Å, respectively. The Eu^{2+} ions are prone to occupy the Ba^{2+} sites in BLSO because the charges of Eu^{2+} and Lu^{3+} ions are different; moreover, the 6-coordinated Eu^{2+} ion (1.17 Å) is bigger than the trivalent Lu^{3+} ion (0.861 Å), but smaller than Ba^{2+} (1.35 Å).

Liu *et al.*[66] thoroughly investigated the structure of BLSO phosphors by refinement of X-ray diffractograms. The structural view along the *c* axis (Fig. 1b) reveals a single layer of the rhombohedral structure, where the bigger octahedral units of LuO_6 are connected in nearly-hexagonal array-sharing corners to the smaller tetrahedral units of SiO_4. The LuO_6 octahedra are distorted in this structure. The O–Lu–O bond angle changes from 85.1° (±8) to 97.1° (±2). The distorted tetrahedral structure of SiO_4 has a Si–O bond length in the range of 1.587 to 1.668 Å, and the O–Si–O bond angles range from 104.4 to 118.2°.

The view along the *b* axis of the layered crystal structure of BLSO (Fig. 1c) displays three barium crystallographic sites – Ba(1), Ba(2), and Ba(3). The crystallographic sites Ba(1) and Ba(2) are arrayed in the chains of interlayer-gaps and connect the Lu–Si–O layers, which have chains of the Ba(3) cationic sites. The Lu^{3+} and Si^{4+} have only one crystallographic site, which is coordinated with six (6) and four (4) oxygens, respectively.

3. Tuning of photoluminescence emission following the strategy of the occupation of multiple crystallographic sites of single-phase phosphors with activators

3.1 Eu^{2+} occupation in multiple crystallographic sites

Single-phase phosphors have broadly and continuously tunable photoluminescence excitation and emission. They have been the most intensively investigated materials in recent years because of their potential for use in a variety of applications at low cost, such as highly efficient solid-state lighting, high-quality color displays, biological sensing, information storage, and labeling.[52,67–73] In order to produce efficient white-light emission, many studies have been focused on presenting strategies for developing novel single-phase phosphors and for optimizing their characteristics. Among them, crystal-site engineering has produced outstanding results. For instance, the green-emitting α_L-Ca_2SiO_4:Eu^{2+} phosphor is tailored to a red-emitting phosphor, while the ordering of SiN_4 and AlN_4 clusters in (CaSr)$SiAlN_3$:Eu^{2+} improves the luminescence intensity.[74,75] Hence, modifying the properties of known phosphors by using crystal-site engineering is a promising approach for developing new phosphors with desirable features.

The host lattice of phosphors has multiple crystallographic sites, thus offering the possibility for tuning luminescence *via* engineering of the surrounding environment of activators. Because of the potential mismatch between the activator and the host cation, the activator will occupy the most suitable crystallographic site.[76,77] This means that increasing the dopant concentration will effectively tune the luminescence to the desired values (in other words, efficient tuning) since the activator ions would be forced to occupy the less suitable cationic sites in the host lattice.[31,77–79] Additionally, cation substitution can force the luminescent center to enter the less appropriate crystallographic sites found within the multiple cationic sites in the host lattice.[76,80–84] For example, in $Sr_{2-x}Ba_xSi_2O_2N_2:Eu^{2+}$ oxynitride phosphors, cation substitution shifts the divalent Eu^{2+} to a non-preferential site, resulting in efficient tuning of the luminescence towards longer wavelengths.[85] In general, cation substitution is highly considered as an efficient strategy to tune photoluminescence excitation and emission to a desired range of the spectral region.[86–89]

A well-known blue-emitting phosphor is $Ba_9Lu_2Si_6O_{24}:Eu^{2+}$ ($BLSO:Eu^{2+}$). Multiple crystallographic sites are available for the occupation with divalent Eu^{2+} ions in the BLSO host lattice, resulting in a variety of color emission. Many investigations have been conducted in order to throw light on the origin of the varied color emission. The emission spectrum has been studied in detail by several researchers by using a variety of techniques, such as room and low temperature photoluminescence spectroscopy and Gaussian fitting.

The team of Yongfu Liu[90] was the first to investigate the anomalous red emission of divalent Eu^{2+}-activated BLSO silicate phosphors. The normalized room-temperature photoluminescence (PLE and PL) spectra of $BLSO:3\%Eu^{2+}$ phosphors (Fig. 2a) show that all the PL spectra display broad-band blue emission, having a maximum at 460 nm with a long tail. The range of the emission spectra peaking at 510 nm is enhanced when the wavelength of excitation (PLE) is tuned from 342 nm to 430 nm. In order to find the reason behind the enhancement towards the longer wavelength region, photoluminescence excitation spectra were recorded at the monitored wavelengths of various emissions, *i.e.* at the peak position (460 nm), in the shoulder enhancement (510 nm), and in the tail (610 nm). It was observed that the photoluminescence excitation spectra became broad when the monitored emission wavelength shifted from 460 to 510 and 610 nm. The recorded spectra reveal various peak positions in the excitation profile for all three monitored emissions. The various excitation and emission profiles suggest that more than one luminescent center should result in this phenomenon.

In order to deeply shed light (provide more details) on the existence of multiple luminescent centers in the BLSO phosphor host lattice, the PLE and PL spectra of $BLSO:3\%Eu^{2+}$ were recorded at low temperature, *i.e.* 77 K (Fig. 2b). Three peaks around 460 nm, 510 nm, and 610 nm were recorded. The PLE spectra monitored at the three different emission peaks were also observed to be significantly different at a temperature of 77 K. The photoluminescence excitation spectrum at a monitored wavelength of 510 nm exhibits a narrow and dominant peak around 430 nm, while two other peaks at 370 and 280 nm are significantly different from those in the broad PLE spectrum recorded at room temperature. These results support the Eu^{2+} occupation in the three different crystallographic sites in BLSO phosphors. In other words, the three different emission peaks are results of Eu^{2+} ions which occupied the three different crystallographic sites in BLSO phosphors.

The origin of these three emission peaks was investigated in detail. The luminescence of the Eu^{2+}-activated BLSO silicate phosphors was compared with the luminescence of Eu^{2+}-doped $Ba_9Sc_2Si_6O_{24}$ (BSSO) and $Ba_9Y_2Si_6O_{24}$ (BYSO), which have the same crystal structure as the BLSO phosphor host lattice. The activated divalent Eu^{2+} ions occupy the Ba^{2+} sites in BSSO and BYSO.[91,92] Green emission with a peak at around 505 nm at RT is recorded in the spectra of both $BSSO:Eu^{2+}$ and $BYSO:Eu^{2+}$ phosphors. The green-color emission at a low temperature consists of two bands, peaking at 460 and 510 nm.[93,94] Although the BLSO phosphors have an identical crystal structure to the BSSO and BYSO phosphors, the Eu^{2+}-doped BLSO phosphors display deep-blue emission (460 nm) at room temperature, which is completely different from the green emission (505 nm) of $BSSO:Eu^{2+}$ and $BYSO:Eu^{2+}$. More interestingly, a new emission band in the red spectral region, having a peak at around 610 nm, was observed at 77 K, which was not recorded in the spectra of the $BSSO:Eu^{2+}$ and $BYSO:Eu^{2+}$ phosphors.

In the host lattice of BLSO phosphors, the average bond length of the 9-coordinated Ba(2) site (2.925 Å) is comparable to that of the 10-coordinated Ba(3) cationic site (2.934 Å), providing, therefore, a similar crystal-field strength to the 5d state of the doped Eu^{2+} ions. The average bond length of the 12-coordinated Ba(1) crystallographic site (3.085 Å) is greater than the bond lengths of the Ba(2) and Ba(3) crystallographic sites. Therefore, the Ba(1) crystallographic site provides a different surrounding environment, like weaker crystal-field strength to the doped Eu^{2+}, by comparison with the Ba(2) and Ba(3) cationic sites. As discussed earlier, the 5d energy level of the divalent Eu^{2+} ions is greatly affected by the surrounding environment, like crystal-field splitting. Hence, the high-energy blue-emission peaking at 460 nm should be ascribed to the doped Eu^{2+} occupying the Ba(1) crystallographic site, which has a weaker crystal-field strength. The green emission at around 510 nm might be attributed to the occupation of the Ba(2) and Ba(3) crystallographic sites by the Eu^{2+} ions, which provide stronger crystal-field strength.

The energy-transfer mechanism can be considered as a possible reason for the appearance of the three different emission peaks. The phenomenon of energy transfer from the divalent Eu^{2+}-doped Ba(1) site to the other available crystallographic sites Ba(2) and the Ba(3) is schematically presented in Fig. 2c. At room temperature, part of the energy from the blue luminescent center (460 nm) is transferred to the green luminescent center (510 nm) using path a. The transfer of energy from both the blue (460 nm) and green (510 nm) luminescent centers to 610 nm was observed at low temperature (77 K), as

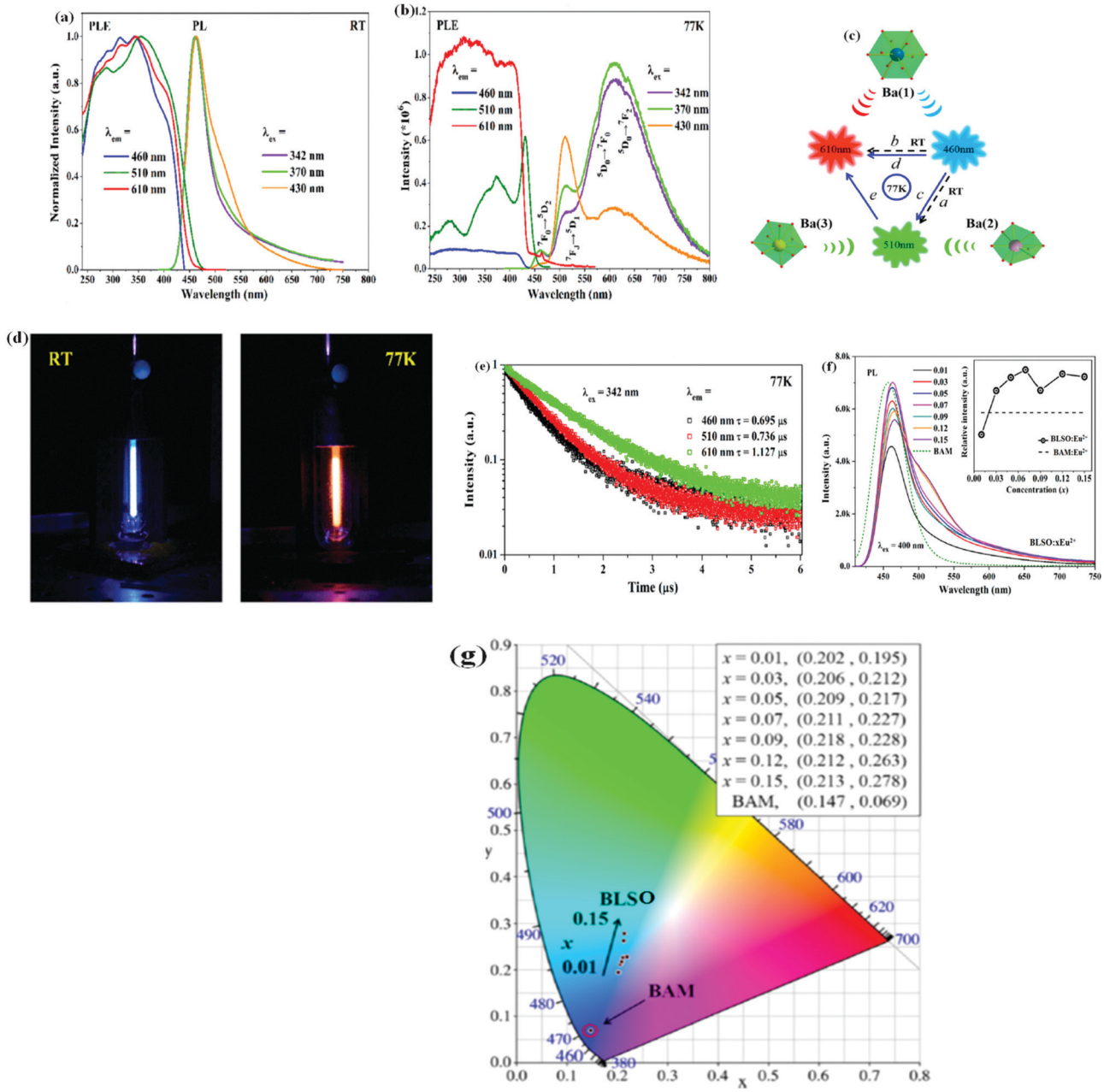

Fig. 2 Features and properties of BLSO phosphors: PLE and PL spectra at (a) room temperature and (b) 77 K, (c) energy-transfer mechanism among the three luminescent centers, (d) digital photographs at room temperature and 77 K, (e) decay curves of the three luminescent centers at 77 K, and (f) photoluminescence emission and (g) CIE chromaticity diagram for various concentrations of Eu^{2+} (x = 0.01–0.15), under 400 nm excitation.[90] (Reproduced with permission from ref. 90, copyright 2016, American Chemical Society.)

shown in paths d and e, respectively. Thus, the low-temperature (77 K) luminescence spectra show an intensive red emission peak around 610 nm. This phenomenon was also observed when the phosphor sample (in powder form) was subjected to liquid nitrogen temperature. The digital photographs of the samples at room and low temperatures are shown in Fig. 2d. The decay-time profiles monitored at the three emission peaks (460, 510, and 610 nm) at 77 K are shown in Fig. 2e. The three different fluorescence decay-time profiles for the three monitored emission peaks confirm the three different luminescent centers of Eu^{2+} in the BLSO phosphors.

The photoluminescence emission and CIE of the BLSO phosphors at various concentrations of Eu^{2+} (x = 0.01–0.15), under 400 nm near-UV light excitation, are plotted in Fig. 2f and g, respectively. The optimized concentration for 460 nm emission is x = 0.07. The emission-peak intensity at 510 nm increases up to x = 0.12. At higher concentrations of Eu^{2+} ions, enhancement of efficient energy transfer to other available crystallographic sites should occur. The tuning of the emission color from 460 nm to longer wavelengths at higher concentrations of the Eu^{2+} ions was also observed (Fig. 2g).

The Eu^{2+} occupation in multiple crystallographic sites was considered as the main reason for enabling the tuning of photoluminescence excitation and emission in the BLSO phosphor host lattice. Although most of the work done was conducted at low temperatures, the understanding of the tuning of PLE and PL at room temperature is of major importance. In our previous work, we studied various cationic substitutions.[33,38] The anomalous tuning from blue to efficient green emission of Eu^{2+} singly doped $Ba_9Lu_2Si_6O_{24}$ (BLSO:Eu^{2+}) silicate phosphors was investigated. The origin of the blue emission was first thoroughly investigated by analyzing the crystal structure of the BLSO phosphor host.

The normalized PLE and PL spectra of BLSO:$x$$Eu^{2+}$ silicate phosphors (for x = 0.05, 0.1–0.6) under various excitations (respective to the corresponding emission peaks) are shown in Fig. 3a. The phosphors with x = 0.05 to 0.3 displayed a high intensity blue-light emission in the range of 400–600 nm, with a long tail towards 700 nm, having a dominant intensity peak around 463 nm. These emission spectra are analogous to those in the previously reported work.[95] The prominent photoluminescence excitation in the UV to near-UV range (peaking at 342 nm) and the high intensity broadband blue emission (peaking at 463 nm) correspond to $4f^5d^1 \rightarrow 4f^7$ allowed transitions.

The emission color was efficiently tuned towards the green-spectral region with the increase of Eu^{2+} content from x = 0.3 to 0.6, although all the prepared phosphors with higher Eu^{2+} concentrations maintained the rhombohedral BLSO phase. The emission spectrum becomes a doublet at the optimized Eu^{2+} concentration (x = 0.3), having two emission peaks below and above the 500 nm emission peak. Further enhancement of the Eu^{2+} content results in a variation of the photoluminescence emission spectrum of the Eu^{2+} doped BLSO phosphor host lattice. The BLSO phosphor with x = 0.6 (Fig. 3b) exhibited broadband green emission, having a dominant peak at 514 nm. The variation produced in the photoluminescence emission spectra of the prepared Eu^{2+}-doped BLSO silicate phosphors supports that there are numerous luminescent centers in the synthesized BLSO host lattice.

The efficient tuning of the emission spectra of the prepared BLSO:Eu^{2+} phosphors from dark blue to efficient green is attributed to the variations in the emission centers among the three available (Ba(1) to Ba(2) and Ba(3)) crystallographic sites. Hence, the shorter wavelength blue emission (peaking at 463 nm) at the lower Eu^{2+} (x = 0.05 to 0.3) concentrations is attributed to the spin allowed $4f^65d^1 \rightarrow 4f^7$ transitions of the activator Eu^{2+} in the first available Ba(1) crystallographic sites owing to the highly preferential occupation of the Ba(1) crystallographic site in the BLSO host lattice with the divalent Eu^{2+}.[93] Upon increasing the concentration of the divalent Eu^{2+} activators in the produced BLSO phosphors host-lattice compositions, the dominant blue-emission peak around

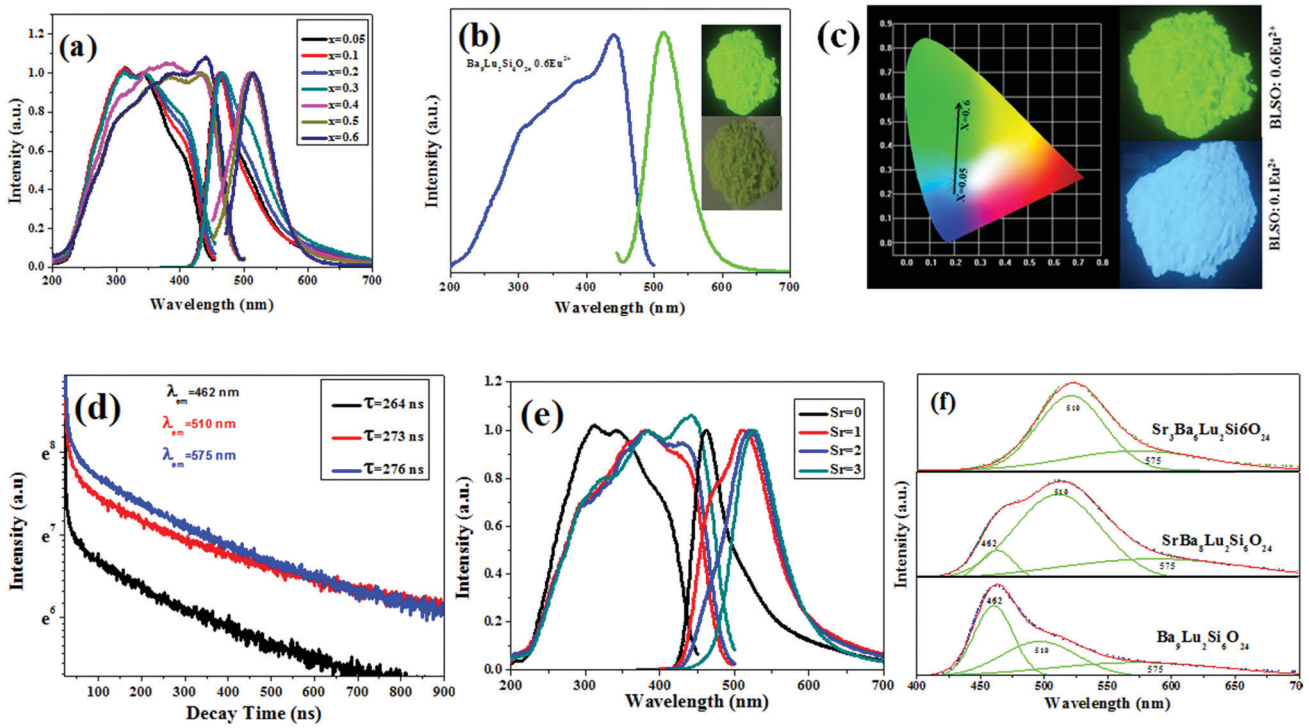

Fig. 3 The photoluminescence properties of BLSO:Eu^{2+} phosphors, such as (a) normalized PLE and PL spectra at room temperature, (b) PLE and PL for 0.6Eu^{2+} with digital photographs under common daylight (photo at the bottom) and under 365 nm UV light (top photo), (c) CIE chromaticity diagram with digital photographs under 365 nm UV light, (d) decay-time profiles and (e) normalized PLE and PL spectra for Sr^{2+}-substituted samples, and (f) deconvolution of the emission spectrum for throwing light on the mechanism of the green-emission enhancement.[33] (Reproduced with permission from ref. 33, copyright 2018, Elsevier.)

463 nm disappears as a result of the concentration quenching of the activator Eu^{2+} in the Ba(1) site in the prepared BLSO phosphor host. The Eu^{2+} concentration in the available non-preferential cationic-sites of Ba(2) and Ba(3) increases with the increase of the x concentration from x = 0.3 to 0.6. The appearing green-emission of the BLSO:Eu^{2+} silicate phosphors should also correspond to $4f^6 5d^1 \rightarrow 4f^7$ transitions in the doped divalent Eu^{2+} ions at the Ba(2) and Ba(3) cationic sites of the BLSO phosphor host.

The efficient color-coordinate tuning, as a response to the concentration of the Eu^{2+} activator in the BLSO phosphors, according to the emission spectra under its corresponding excitation, is shown in Fig. 3c. The digital photographs of the prepared $Ba_9Lu_2Si_6O_{24}$:0.1Eu^{2+} and $Ba_9Lu_2Si_6O_{24}$:0.6Eu^{2+} phosphors (*i.e.* the low and high Eu^{2+} concentrations, respectively) under 365 nm UV light irradiation are shown on the right-hand side of Fig. 3c, which confirms the color-coordinate tuning with increasing concentration of Eu^{2+} ions. When divalent Eu^{2+} ions are accommodated in the Ba^{2+} crystallographic sites of the BLSO:$x$$Eu^{2+}$ phosphor host lattice (for x = 0.05, 0.1, 0.2, 0.3, 0.4, 0.5, and 0.6), the emission color shifts from blue to green. This qualifies these color-tunable BLSO:$x$$Eu^{2+}$ phosphors as prominent candidates for white light-emitting diodes (white LEDs), excitable over a longer wavelength range, like UV, near UV, and blue light.

The presence of the three luminescent centers was also verified by recording the fluorescence decay time. The obtained results (Fig. 3d) show three different decay components, associated with the Eu^{2+} occupation in the three crystallographic sites of the BLSO phosphor host lattice.

In order to suppress concentration quenching, various substitutions with cations with smaller ionic radii, such as Sr^{2+} and Ca^{2+}, were attempted to tune photoluminescence to a region of longer wavelengths. The substitution with the former ion leads to the tuning of photoluminescence excitation and emission spectra towards a longer wavelength region by shifting the activator Eu^{2+} to the next available crystallographic sites, *i.e.* the Ba(3). The crystallographic site Ba(3) has a different surrounding environment, such as a different coordination number and bond length with oxygen, compared to the Ba(1) site, which tunes photoluminescence excitation and emission to a longer wavelength region, whose normalized graphs are plotted in Fig. 3e.

The deconvolution of the emission spectrum for shedding light on the mechanism of tuning luminescence is shown in Fig. 3f. The emission spectrum of BLSO was perfectly deconvoluted into three Gaussian peaks. The peak at 510 nm is related to the Eu^{2+} occupation in the Ba(3) crystallographic sites, which enhances with increasing Sr^{2+}-ion concentration. The substitution of the Ca^{2+} ion, with a smaller ionic radius, for Ba^{2+} efficiently broadens the emission spectra of BLSO:Eu^{2+} silicate phosphors.

The normalized PLE and PL spectra of the BLSO:0.2Eu^{2+} with various contents of Ca^{2+} are shown in Fig. 4a. Under 343 nm UV light excitation, the sample with Ca^{2+}-free BLSO:0.2Eu^{2+} emits strong blue light ranging from 400 to 700 nm, peaking at 462 nm. The substitution of Ca^{2+} for Ba^{2+} in $Ca_xBa_{(9-x)}Lu_2Si_6O_{24}$:0.2$Eu^{2+}$ (CBLSO:0.2Eu^{2+}) phosphors broadens the emission spectrum, which covers the blue, green, and yellow regions of the visible spectrum.

Gaussian fitting was applied in the emission spectra of both the Ca^{2+}-free and Ca^{2+}-doped BLSO:Eu^{2+} phosphors (Fig. 4b). The emission spectra were deconvoluted into three components (centered at 465, 496, and 573 nm), suggesting three different luminescent centers in the prepared BLSO phosphors. The lower-wavelength blue-emission peaking at 465 nm is assigned to the preferable occupation of the Ba(1) crystallographic site with Eu^{2+} ions, and the higher-wavelength peaks of 496 and 573 nm are attributed to the occupation of the Ba(3) and Ba(2) cationic sites with Eu^{2+} ions.

By introducing a smaller ionic radius Ca^{2+} to replace Ba^{2+}, changes in the emission spectra towards a longer wavelength region are observed (Fig. 4b). The longer wavelength part of the emission spectrum (with peaks at 496 and 573 nm) is intensified; therefore, the emission spectra are broadened and cover a great part of the visible region. The enhancement of the longer wavelength peaks is ascribed to the Eu^{2+} occupation of Ba(3) and Ba(2) crystallographic sites. The ionic radius of the Ca^{2+} ion is less than those of Eu^{2+} and Ba^{2+}. As a result, Ca^{2+} should occupy the Ba(1) site, which results in the Eu^{2+} ion occupying the Ba(3) and Ba(2) cationic sites.

The substitution of Ca^{2+} for Ba^{2+} in BLSO phosphors not only broadens the emission spectrum to the desired wavelengths but also enhances thermal stability to reach the desired value. The photoluminescence emission spectra of BLSO:Eu^{2+} and CBLSO:Eu^{2+} measured at various temperatures (25–150 °C) are shown in Fig. 4c and d, respectively. The luminescence intensity of both the BLSO and CBLSO decreases with the increase in temperature. However, the color of the emission remains unchanged with the increase in temperature. The dependence of the maximum photoluminescence intensity on temperature for x = 0 and 1.5 is shown in the plot of Fig. 4e. The stability against temperature is increased by increasing the Ca^{2+} content in CBLSO:0.2Eu^{2+} phosphors. This is attributed to two reasons. When a contraction in the unit volume occurs, the interactions between the divalent Eu^{2+} dopant and O^{2-} (which are the crystal-field effects and nephelauxetic effects for the 5d orbital of Eu^{2+} activators) vary. In addition, when the content of Ca^{2+} ions is increased, various surrounding environments for the divalent Eu^{2+} dopants are obtained on account of the movement of the activator Eu^{2+} to the Ba(2) and Ba(3) sites from the Ba(1) site.

The electroluminescence emission spectrum of a fabricated white-LED lamp under 365 nm UV light is plotted in Fig. 4f. High-quality white light was obtained, with CIE chromaticity-coordinates as (0.380, 330), located nearly in the ideal white light region, which could be effectively tuned to the desired color region by varying the concentration of the divalent Ca^{2+}, Eu^{2+}, and Mn^{2+} cations. The white light-emitting diode lamp (LED lamp excited at 365 nm) shown in the inset of Fig. 4f was fabricated by combining a CBLSO:Eu^{2+}/Mn^{2+} phosphor with a commercial 365 nm UV chip. Efficient warm white light was generated (inset of Fig. 4f).

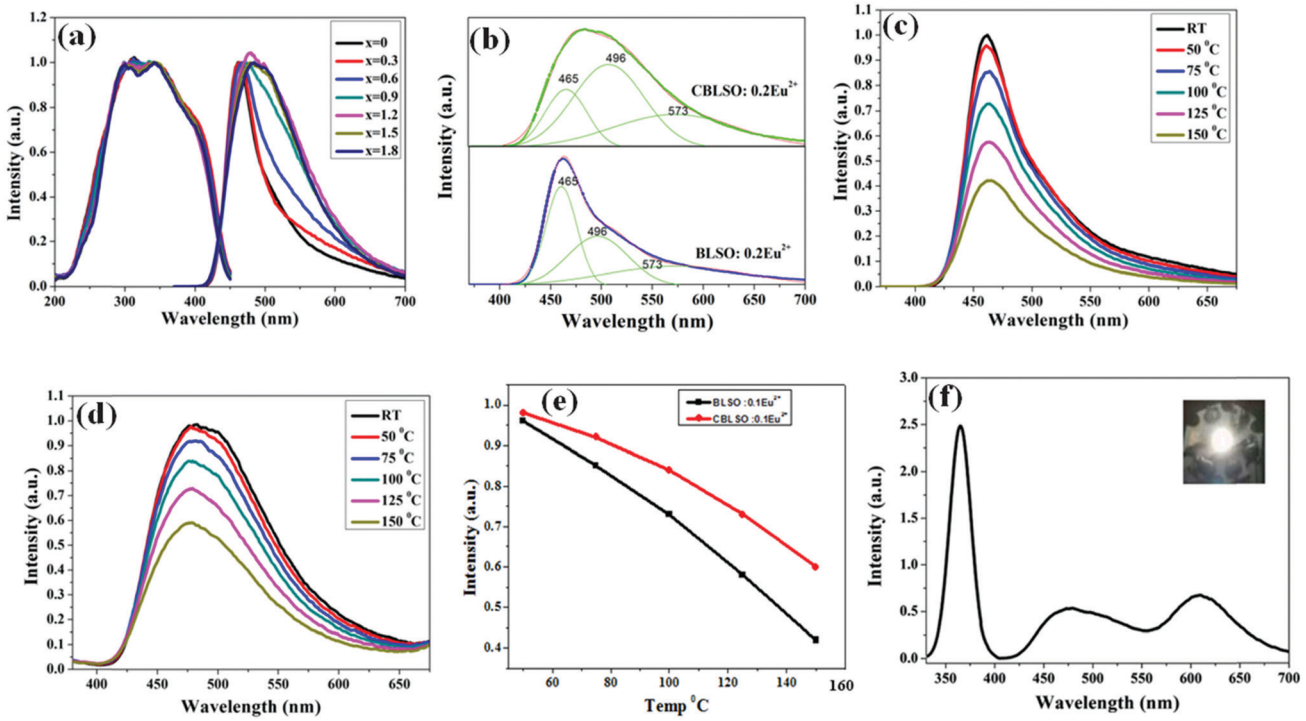

Fig. 4 Influence of Ca^{2+} substitution on the photoluminescence properties of BLSO:Eu^{2+} phosphors, (a) normalized PLE and PL spectra, (b) deconvolution of the emission spectrum for shedding light on the mechanism of the enhancement of the longer wavelength peaks, (c, d and e) temperature dependences of PL of BLSO and CBLSO and (f) electroluminescence emission spectrum with a digital photograph of the fabricated LED device in the inset.[38] (Reproduced with permission from ref. 38, copyright 2017, American Chemical Society.)

3.2 Ce^{3+} occupation in multiple crystallographic sites

Similar to the divalent Eu^{2+} ion, the trivalent Ce^{3+} ion also manifests 5d–4f transitions where the 5d state is very sensitive to the surrounding environment of the phosphor host lattice. The Ce^{3+} occupation in various multiple crystallographic sites of the BLSO host lattice favors the tuning of PLE and PL spectra over a broad range in the visible spectral region.

Yongfu Liu[66] and co-workers developed efficient and highly stable green-emitting BLSO:Ce^{3+} phosphors. A highly efficient green-emitting Ce^{3+}-doped BLSO orthosilicate phosphor was produced by using a traditional solid-state method at a comparatively low reaction temperature of 1400 °C. The optical characteristics were comparable to those of most nitride phosphors, which, nonetheless, require high temperatures and a suitable atmosphere for their synthesis. The produced Ce^{3+}-doped BLSO phosphors showed a high internal-quantum efficiency of 82% under 400 nm near-UV light excitation. Furthermore, these green-emitting phosphors exhibited superior thermal stability, *i.e.* a 94% remaining intensity at a high temperature of 160 °C, compared to the intensity at room temperature. The crystal structure and luminescence characteristics were thoroughly investigated in order to shed light on the high intensity and the excellent thermal stability of the green color emission of the Ce^{3+}-activated BLSO phosphors.

The photoluminescence excitation and emission spectra of the optimized $Ba_9Lu_{1.89}Ce_{0.11}Si_6O_{24}$ phosphor are shown in Fig. 5a. The broadband PLE spectrum at the monitored-emission wavelength of 490 nm ranges from 200 nm to 450 nm, with a dominant peak around 400 nm. The broadband excitation corresponds to Ce^{3+} occupying Lu^{3+} crystallographic sites, which have almost the same energy range as the Y^{3+}-based silicate of the same family ($Ba_9Y_2Si_6O_{24}$:Ce^{3+}).[96] The influence of the Ce^{3+} concentration on the luminescence spectra of $Ba_9Lu_{2-x}Ce_xSi_6O_{24}$ (for x = 0.01–0.15) phosphors under 400 nm near-UV light excitation is plotted in the inset of Fig. 5a. The photoluminescence intensity gradually increases upon increasing the concentration of Ce^{3+} ions up to x = 0.11. A further increase of Ce^{3+} concentration ($x > 0.11$) decreases the luminescence intensity due to concentration quenching.

Under 400 nm excitation, the optimized $Ba_9Lu_{1.89}Ce_{0.11}Si_6O_{24}$ phosphor displays a dominant cyan emission peaking at 490 nm with a broad width of 118 nm (4519 cm^{-1}), which corresponds to the spin-allowed transition from the 5d-excited state to $^2F_{5/2}$ and $^2F_{7/2}$ ground states of Ce^{3+} ions. The emission spectrum was deconvoluted into two Gaussian peaks (dashed lines), with the dominant peaks at 476 nm (20 992 cm^{-1}) and 526 nm (19 017 cm^{-1}). The energy difference is 1975 cm^{-1}, which is nearly equivalent to the theoretical energy difference of Ce^{3+} ion ground-state splitting (separation between the $^2F_{5/2}$ and $^2F_{7/2}$ levels).

The PLE (λ_{max} = 400 nm) and PL (λ_{max} = 490 nm) spectra of the Ce^{3+}-doped BLSO phosphors (Fig. 5a) show a redshift compared to the PLE (λ_{max} = 394 nm) and PL (λ_{max} = 480 nm) in the yttrium series (BYSO).[96] The Y–O bond length in the YO_6 octahedra of the BYSO phosphors is greater than the Lu–O bond length in the LuO_6 octahedra of the BLSO phosphors. Thus, the redshift is attributed to the shorter Lu–O bond length in the LuO_6 octahedra

in the BLSO phosphors. The observed redshift is an important feature for enhancing the red-light component in order to improve the color rendering index when Lu^{3+}-based (BLSO:Ce^{3+}) silicate phosphors are used in near-UV (NUV) pumped w-LEDs.

The excitation band, ranging from 200 to 350 nm and peaking at 330 nm (Fig. 5a), is attributed to the Ce^{3+}occupation in Ba^{2+} crystallographic sites, suggested by the fact that this excitation band is positioned near the energy range of both $Ba_9Y_2Si_6O_{24}$:Ce^{3+} (BYSO:Ce^{3+}) and $Ba_9Sc_2Si_6O_{24}$:Ce^{3+} (BSSO:Ce^{3+}).[96–98] The excitation band is deconvoluted into three Gaussian bands at low temperature (77 K), ascribed to the Ce^{3+} occupation in the three crystallographic sites of Ba^{2+} ions.[96,97] The 5d-excited state of the doped Ce^{3+}/Eu^{2+} ions is strongly affected by the influence of crystal-field splitting.

Eqn (1) shows the relationship between crystal-field splitting (Dq) and bond length (R):

$$\mathrm{Dq} = \frac{Ze^2r^4}{6R^5} \quad (1)$$

where Z represents the anionic charge, r is the radius of the 5d wave function, e is the charge of the electron, and R denotes the bond length of the occupied crystallographic site with oxygen.[99] Therefore, the shorter wavelength peaks of excitation are associated with the Ce^{3+} ion occupation in Ba^{2+} crystallographic sites. On the other hand, the longer wavelength-excitation band peaking at 400 nm is ascribed to the Ce^{3+} occupation in Lu^{3+} crystallographic sites owing to the stronger crystal-field splitting and the shorter Lu–O bond length compared to the longer Ba–O bond length and the corresponding weaker crystal-field splitting.

All the prepared samples of Ce^{3+}-doped BLSO phosphors were colorless under ordinary daylight. Under 365 nm UV light excitation, the optimized sample of BLSO:0.11Ce^{3+} displayed an efficient green color (Fig. 5b). In order to demonstrate the photoluminescence of these phosphors in a more striking way, the Chinese Academy of Sciences (CAS) prepared a yellow ceramic board where the logo and the letters CNITECH were

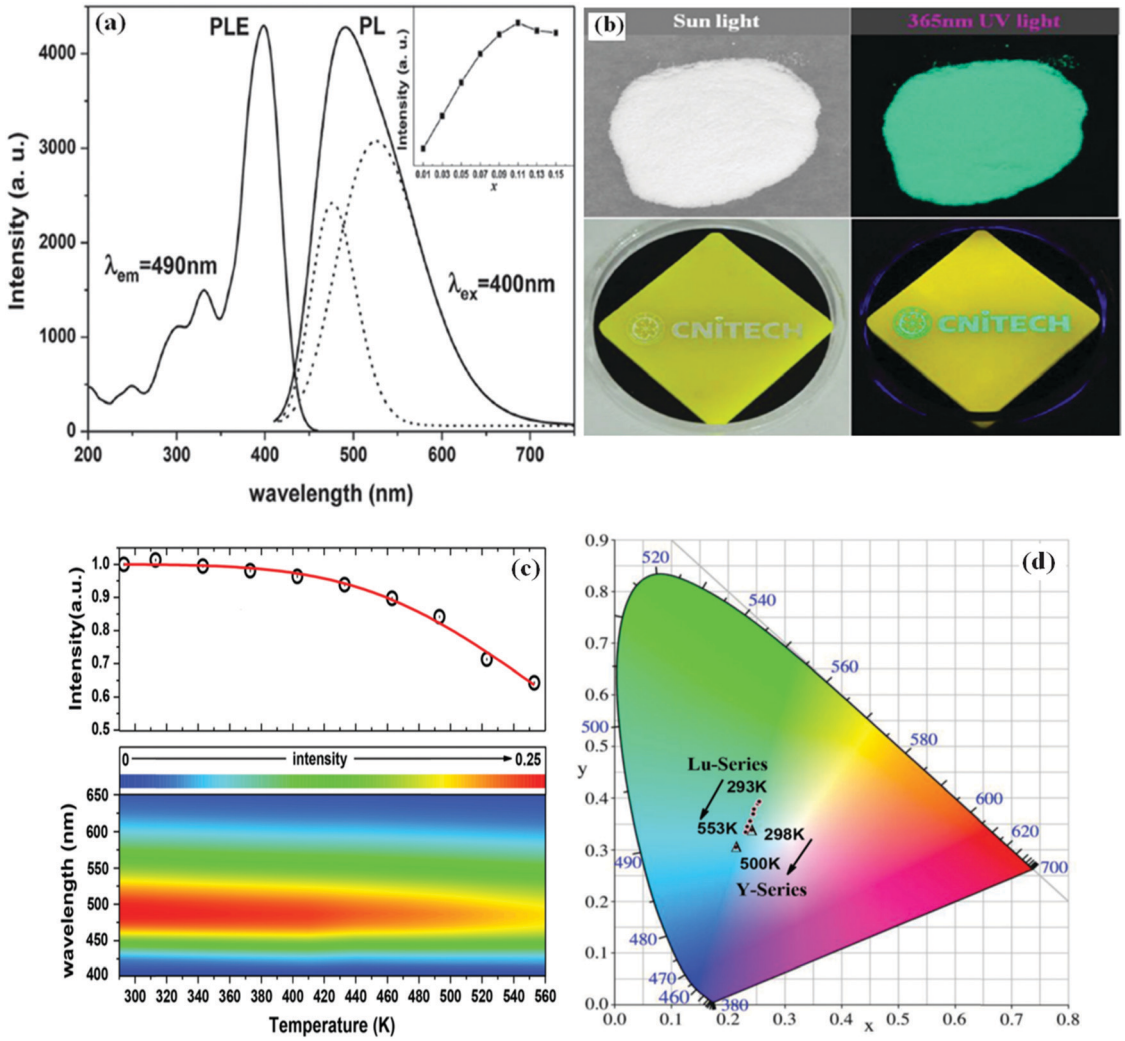

Fig. 5 (a) PLE and PL spectra of the optimized $Ba_9Lu_{1.89}Ce_{0.11}Si_6O_{24}$ phosphor and (inset) the influence of Ce^{3+} on the relative intensity of $Ba_9Lu_{2-x}Ce_xSi_6O_{24}$, (b) the digital photographs under ordinary daylight and 365 nm UV light, (c) the temperature dependence of the intensity and color, and (d) the CIE color coordinate diagram.[66] (Reproduced with permission from ref. 66, copyright 2015 Wiley.)

written (Fig. 5b). The prepared yellow ceramic board was filled with the colorless phosphor, which became green under 365 nm UV light (Fig. 5b).

The thermal stability of phosphors is an important parameter for evaluating their suitability in practical applications.[100–102] The stability of the Ce^{3+}-doped BLSO phosphors was measured. The photoluminescence intensity of the emission spectrum of the optimized phosphor sample was measured within a wide temperature range, from 25 to 160 °C. The measured photoluminescence emission intensity at various temperatures was normalized with the emission intensity at room temperature and it is plotted in the top diagram of Fig. 5c. At the highest tested temperature of 160 °C (433 K), the emission intensity was 93.8% of the emission intensity at room temperature. This performance is significantly higher than that of well-known nitride phosphors, which is 80–90% at 150 °C (with respect to the PL intensity at room temperature).[103]

When the trivalent Ce^{3+} occupied the smaller ionic radius Lu^{3+} site, compared with the larger ionic radius Ba^{2+} sites, the Ce^{3+} activated BLSO phosphors showed remarkable temperature stability. Compared with Ce^{3+} and Eu^{2+} occupying the larger ionic radius Ba^{2+} crystallographic sites, the smaller ionic radius Lu^{3+} offers stronger crystal field splitting to the activated Ce^{3+} ions, resulting in enhanced thermal stability.[47,48,104] Furthermore, the higher activation energy (by 0.382 eV) resulting from the more rigid structure of the corner-sharing SiO_4–LuO_6–SiO_4 layers might be attributed to the reduced thermal deterioration in the case of Ce^{3+} occupied Lu^{3+} in BLSO phosphors.[46]

Besides displaying superior thermal stability, the green-emitting BLSO:Ce^{3+} phosphors also exhibit excellent stability of their luminescence color. The results shown at the bottom of Fig. 5c show that when the temperature increases from 293 to 553 K, only a slight blue shift of around 5 nm occurs. More interestingly, the cyan-color emission is shifted from (0.2552, 0.3938) to (0.2301, 0.3345), as illustrated in the CIE coordinate diagram (Fig. 5d). The apparent blue shift is attributed to the expansion of the unit-cell volume on account of the temperature increase. Nevertheless, the Lu^{3+}-based phosphors (BLSO:Ce^{3+}) are still greener than the Y^{3+}-based phosphors (BYSO:Ce^{3+}).[96]

The Ce^{3+} occupation in various crystallographic sites of BLSO leads to the emission of various colors. This offers the possibility of producing a broadband spectrum in the visible region, suitable for efficient white-light illumination. Yongfu Liu[105] and co-workers, *via* both experimental and theoretical approaches, developed a broadband cyan-emitting Ce^{3+}-doped BLSO phosphor which covers both the blue and the green color emission of the visible-light region. The produced BLSO:Ce^{3+} phosphor demonstrates a broadband excitation spectrum, having a peak at 400 nm, which has a perfect matching to a near-ultraviolet (NUV) emitting chip. Additionally, it shows high photoluminescence quantum yields (PLQYs), more than 90% at room temperature, and excellent stability against temperature with a small reduction of only 3% at 150 °C.

In order to shed light on the high internal-quantum efficiency and the excellent thermal stability of the Ce^{3+}-doped BLSO phosphors, various features, like their optical band-gap and luminescence characteristics, were investigated in detail. The phosphor host lattice usually needs a wide band-gap to efficiently occupy the energy levels of doping luminescent ions, like activators. In order to ensure that the proposed BLSO-phosphor host lattice has a wide band-gap, wide enough to accommodate the 4f–5d transition of Ce^{3+} dopants, the electronic-band structure of the pure BLSO was measured by applying the approach of density functional theory (DFT) using VASP. The electronic-band structure of the BYSO-phosphor host lattice was also calculated for the purpose of comparison. The top of the valence band (VB) is at the Γ point, while the bottom of the conduction band (CB) is within the *F*–*Z* region, according to the electronic band structure of the BLSO-phosphor host lattice (Fig. 6a). The results also manifest that the CB minimum and VB maximum were not observed at the same *k*-point, suggesting that the BLSO host lattice has an indirect band-gap. More interestingly, the calculated band-gap value of the BLSO host was observed to be 4.62 eV, which supports that the BLSO is an efficient host lattice for accommodating various luminescent ions within its wide band-gap. The band-gap of the BYSO host lattice (Fig. 6b) displays an indirect band-gap behavior (of 4.74 eV), which is similar to the electronic band structure of the BLSO-phosphor host lattice.

Luminescence characteristics, such as diffuse reflectance spectra (DR spectra), low- and room-temperature photoluminescence, and fluorescence decay time, can throw light on the Ce^{3+} occupation in various available crystallographic sites. The DR spectra in Fig. 6c suggest that Ce^{3+} results in intensive absorption peaks in the range of 330 nm to 400 nm in BLSO:xCe^{3+} phosphors (where x = 0.01–0.15). Similarly, the PLE spectra in Fig. 6d and e show broad excitation bands, with dominant peaks at around 400 nm and 330 nm, respectively. The PLE spectra, ranging from 350 nm to 450 nm and with a peak at 400 nm (which matches well with the near-UV (NUV) emission wavelength of a light-emitting chip), are ascribed to the Ce^{3+} occupation in Lu^{3+} crystallographic sites.[66]

The relative integrated intensities of the Ce^{3+} occupying Lu^{3+} sites were recorded under 400 nm excitation. The results, plotted in the inset of Fig. 6c, show that the optimized concentration of Ce^{3+} is x = 0.11. The PL spectrum of the optimized phosphor is presented in Fig. 5d, which exhibits a broad band having a maximum at 490 nm with a broad FWHM of 118 nm (4519 cm^{-1}). This broadband emission spectrum is attributed to the 5d–4f transition of the Ce^{3+} dopant. The ground state of Ce^{3+} ions is split into $^2F_{5/2}$ and $^2F_{7/2}$ with a theoretical energy difference of 2000 cm^{-1}, due to spin–orbit interaction. The emission band illustrated in Fig. 6d was well fitted with two Gaussian bands as illustrated using dashed lines, peaking at 476.37 nm (20 992 cm^{-1}) and 525.85 nm (19 017 cm^{-1}), with an energy separation of 1975 cm^{-1}, which is very close to the theoretical value (2000 cm^{-1}) of energy separation of the $^2F_{5/2}$ and $^2F_{7/2}$ energy levels.

Compared with the photoluminescence characteristics (λ_{ex} = 394 nm, λ_{em} = 480 nm) of the Ce^{3+}-doped BYSO phosphors,[96] the PLE (λ_{ex} = 400 nm) and PL (λ_{em} = 490 nm) of BLSO show a

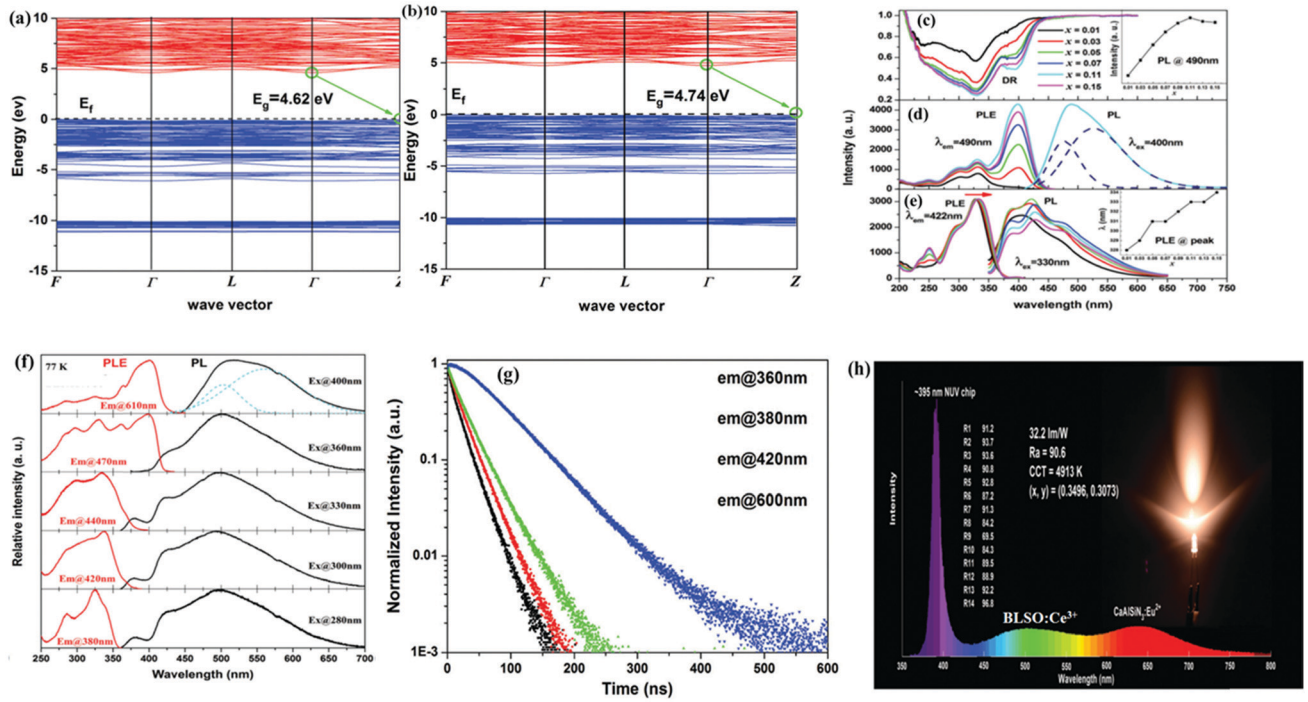

Fig. 6 Electronic-band structures of (a) BLSO and (b) BYSO; (c) DR, (d) PLE and PL spectra of Ce^{3+} occupying Lu^{3+} crystallographic sites; (e) PLE and PL spectra of Ce^{3+} occupying the three different Ba^{2+} sites; (f) PLE and PL spectra of BLSO:11%Ce^{3+} at 77 K at various excitation and emission wavelengths; (g) room-temperature decay-time profiles under 330 nm excitation and monitored at various emission wavelengths; and (h) electroluminescence emission spectrum and digital photograph of the fabricated LED.[105] (Reproduced with permission from ref. 105, copyright 2017 Royal Society of Chemistry.)

redshift. The lowest 5d state of Ce^{3+} ions is greatly influenced by the surrounding environment like crystal-field splitting (*Dq*). Thus, the red shifting that appears in the case of the Ce^{3+}-doped BLSO-phosphor host is ascribed to the enhancement of crystal-field splitting. The characteristic crystal-field splitting was given by eqn (1). Consequently, the value of *r* is proportional to the distortion of the LuO_6 or YO_6 polyhedron in the BLSO and BYSO phosphor host lattices. Based on the values of the Lu–O (2.162–2.223 Å) and Y–O (2.190–2.255 Å) bond-lengths, the distortion of the LuO_6 octahedron (2.82%) in the case of the BLSO is bigger than that of the YO_6 octahedron (1.60%) in the case of BYSO phosphors. This shows that the value of *r* is increased in the case of BLSO phosphors.[66] Accordingly, the combination of the variations of both the parameters, which is the decrease of *R* and the increase of *r* in BLSO, leads to an enhancement of *Dq* around Ce^{3+} ions. This decreases the lowest 5d-energy level and results in a redshift in the PLE and PL spectra of the synthesized BLSO silicate phosphors. More interestingly, the larger distortion of LuO_6, compared to YO_6, leads to a wider emission with FWHM = 120 nm in BLSO than the emission of BYSO (FWHM = 110 nm). The observed redshift would be beneficial for enhancing the red-color component and for increasing the color-rendering index when a broad-band cyan emitting BLSO:Ce^{3+} phosphor is used in NUV pumped white-LEDs.

The photoluminescence excitation that is in the range of 200–350 nm with a dominant peak at 330 nm, depicted in Fig. 6e, is ascribed to the Ce^{3+} occupation in Ba^{2+} crystallographic sites.[66,106] These excitation peaks are located near the energy range of both BYSO:Ce^{3+} and BSSO:Ce^{3+} phosphors.[97,98,107] The low-temperature emission spectrum of the previously reported BYSO:Ce^{3+} phosphors was deconvoluted into three bands, attributed to the Ce^{3+} accommodation in the three crystallographic sites of Ba^{2+} in the host lattice.[96] The phosphors having a nominal composition of BLSO:Ce^{3+} phosphors, where the trivalent Ce^{3+} substitutes only Lu^{3+} (in the chemical composition), show both the emission bands owing to Ce^{3+} occupying the Ba^{2+} and Lu^{3+} sites. This validates that Ce^{3+} ions are located at both the Ba^{2+} and Lu^{2+} crystallographic sites simultaneously.

A thorough outlook on the PLE spectrum monitored at 490 nm emission wavelength suggests that the lower-wavelength excitation (Fig. 6d) is ascribed to the Ce^{3+} accommodation in the divalent Ba^{2+} crystallographic sites in the case of low concentrations of Ce^{3+} (x = 0.01 and 0.03). This low-wavelength excitation (330 nm) is not enhanced at higher concentrations of Ce^{3+} (x = 0.05–0.15) that are related to the longer wavelength excitation peak (400 nm) attributed to the Ce^{3+} occupation in Lu^{3+} crystallographic sites. This phenomenon is ascribed to the fact that Ce^{3+} ions are first accommodated in the Ba^{2+} crystallographic sites at lower concentrations of Ce^{3+} ions. When the concentration of Ce^{3+} is increased, the crystal lattice does not favor further Ce^{3+} occupation in Ba^{2+} crystallographic sites, and therefore, the preferred site for Ce^{3+} activators is that of the trivalent Lu^{3+}. This shows that the imbalance of the local charge produced by

the placement of the trivalent Ce^{3+} in divalent Ba^{2+} crystallographic sites cannot be tolerated by the host lattice of the phosphors at a higher concentration of the doping Ce^{3+} ions.

The photoluminescence excitation (PLE) spectrum at a monitored emission wavelength of 422 nm and at various emission peaks, presented in Fig. 6e, manifests a redshift from 328 nm for x = 0.01 (lowest concentration) to 334 nm for x = 0.15 (highest concentration). A similar trend of redshift in the PLE spectra was also observed in the case of Ce^{3+}-doped BSSO phosphors with increasing concentration of Ce^{3+}. The redshift was attributed to reabsorption between Ce^{3+} occupying the three crystallographic sites of Ba^{2+}. The same phenomenon was also observed in Ce^{3+} occupying Ba^{2+} and Lu^{3+} crystallographic sites ascribed to the overlapping of the emission of Ce^{3+} occupying Ba^{2+} sites with the excitation of Ce^{3+} occupying Lu^{2+} sites (Fig. 6d and e). Hence, a broad emission band of Ce^{3+} occupying Ba^{2+} sites, with various peaks, was observed under low-wavelength excitation (330 nm) (Fig. 6e).

The transfer of energy from Ce^{3+} occupying Ba^{2+} to Ce^{3+} occupying Lu^{3+} sites was confirmed by the low-temperature (77 K) PLE and PL spectra in Fig. 6f. The results in Fig. 6f with the three various excitation peaks at 280, 330, and 360 nm support the Ce^{3+} occupation in the available three different crystallographic sites of Ba^{2+}. When the photoluminescence excitation wavelength was increased from 280 to 330 and 360 nm (PLE of Ce^{3+} located in Ba^{2+} sites), a longer wavelength emission (PL of Ce^{3+} occupying Lu^{3+} sites) was observed. Similarly, a lower-wavelength excitation spectrum (PLE of Ce^{3+} located in Ba^{2+} sites) was obvious at the monitored emission wavelength of the Ce^{3+} occupying the Lu^{3+} sites. These findings further validate the existence of energy transfer from the doped Ce^{3+} located in Ba^{2+} to Ce^{3+} located in Lu^{3+} crystallographic sites. Moreover, the low-temperature luminescence, plotted in Fig. 6f, manifests a redshift of 28 nm, attributed to the contraction of unit-cell volume at low temperatures.

The low-temperature (77 K) photoluminescence decay-time curves of the Ce^{3+}-activated BLSO phosphors were measured at monitored emission wavelengths of 360, 380, 420 (emission of Ce^{3+} occupying Ba^{2+} sites), and 600 nm (emission of Ce^{3+} accommodated in Lu^{3+} crystallographic sites). Under 330 nm excitation (PLE of Ce^{3+} occupying Ba^{2+} sites), the decay times (Fig. 6g) of both the Ce^{3+} occupying Ba^{2+} and the Ce^{3+} occupying Lu^{3+} sites deviate from the single exponential model, but efficiently fit in the double exponential function. The obtained results suggest that the decay times monitored at 360, 380, and 420 nm emission wavelengths reveal a slow-decay component, ranging from 24.1 to 37.0 ns, which is consistent with the typical slow-decay component of the low-wavelength emission from the UV to blue color. Similarly, the decay-time profile at a monitored emission wavelength of 610 nm shows a slow decay component of around 60.6 ns, which is similar to the decay time of a longer wavelength emission in the green color range of the visible spectral region. The observed fast decay time of the shorter wavelength emission of the Ce^{3+} occupying Ba^{2+} sites and the slow decay time of the longer wavelength emission of the Ce^{3+} occupying Lu^{3+} crystallographic sites also confirm the energy transfer from the Ce^{3+} occupying Ba^{2+} to Ce^{3+} occupying Lu^{3+} crystallographic sites.

A white LED was fabricated by coating the optimized BLSO:Ce^{3+} and a commercially available $CaAlSiN_3$:Eu^{2+} red-emitting phosphor on a 395 nm emitting near-UV LED chip to evaluate the performance of the Ce^{3+}-doped BLSO phosphors in white LEDs for commercial applications of efficient white light emitting sources for general illumination. The electroluminescence emission spectrum along with optical characteristics of the fabricated white LED is shown in Fig. 6h. Efficient white light was obtained with a high CRI value of 90.6 and a low CCT at around 4913 K. The white light showed (0.3496, 0.3730) for CIE (x, y) color coordinates at an open circuit of 20 mA. These excellent characteristics reveal that the single and broadband cyan-emitting BLSO:Ce^{3+} phosphors, in contrast to multi-color blue and green phosphors, result in high-quality white light. More interestingly, the cyan/red-emitting phosphor-converted white LED leads to high luminous efficiency, which reached a value of 32.2 lm W^{-1}, which is the maximum value for multiple blue/green/red phosphors coated on near-UV LED chips.

3.3 Bi^{3+} occupation in multiple crystallographic sites

Similar to various rare-earth (RE) ions (activators), such as the Eu^{2+} and Ce^{3+} that have a 5d–4f spin-allowed transition, bismuth (Bi^{3+}) also has ns^2-type luminescent centers, which are sensitive to the surrounding environment governed by the crystal field of the host lattice. It exhibits tunable broadband emission, ranging from the UV to visible and near-infrared spectral regions, as a result of the $6s6p$–$6s^2$ transition.[108,109] Y. Guo[110] and his team reported on the luminescence tuning and crystal-site engineering of Bi^{3+}-activated BLSO phosphors. They obtained tunable white-light emission from single-phase phosphor-converted white LEDs taking into account the Bi^{3+} occupation in multiple crystallographic sites.

The photoluminescence characteristics measured suggest that the prepared Bi^{3+}-doped BLSO phosphors display different luminescence features under various excitations. The photoluminescence excitation that is monitored at 410/485 nm and photoluminescence emission under 335/370 nm excitation of the BLSO:0.05Bi^{3+} phosphors depicted in Fig. 7a show that there is no luminescence in the case of the non-doped sample. Thus, the obtained luminescence characteristics should be attributed to Bi^{3+} ions doped in BLSO phosphors.

The sample BLSO:0.05Bi^{3+} exhibits broadband blue emission in the range of 380–500 nm with a dominant peak at 410 nm under 370 nm UV light excitation. By monitoring the emission at 410 nm, this phosphor exhibits double-band excitation, peaking at 335 and 370 nm with a long tail in the high wavelength region. Under 335 nm UV light irradiation, the trivalent Bi^{3+}-activated BLSO phosphors show broadband emission in the range of 350–650 nm, having various emission peaks, at 365, 410, and 485 nm. The excitation spectrum measured at a monitored emission wavelength of 485 nm (Fig. 7b) can be well fitted into three asymmetric absorption peaks located at around 3.905 eV (317.5 nm), 3.807 eV (325.7 nm), and 3.616 eV (342.9 nm).

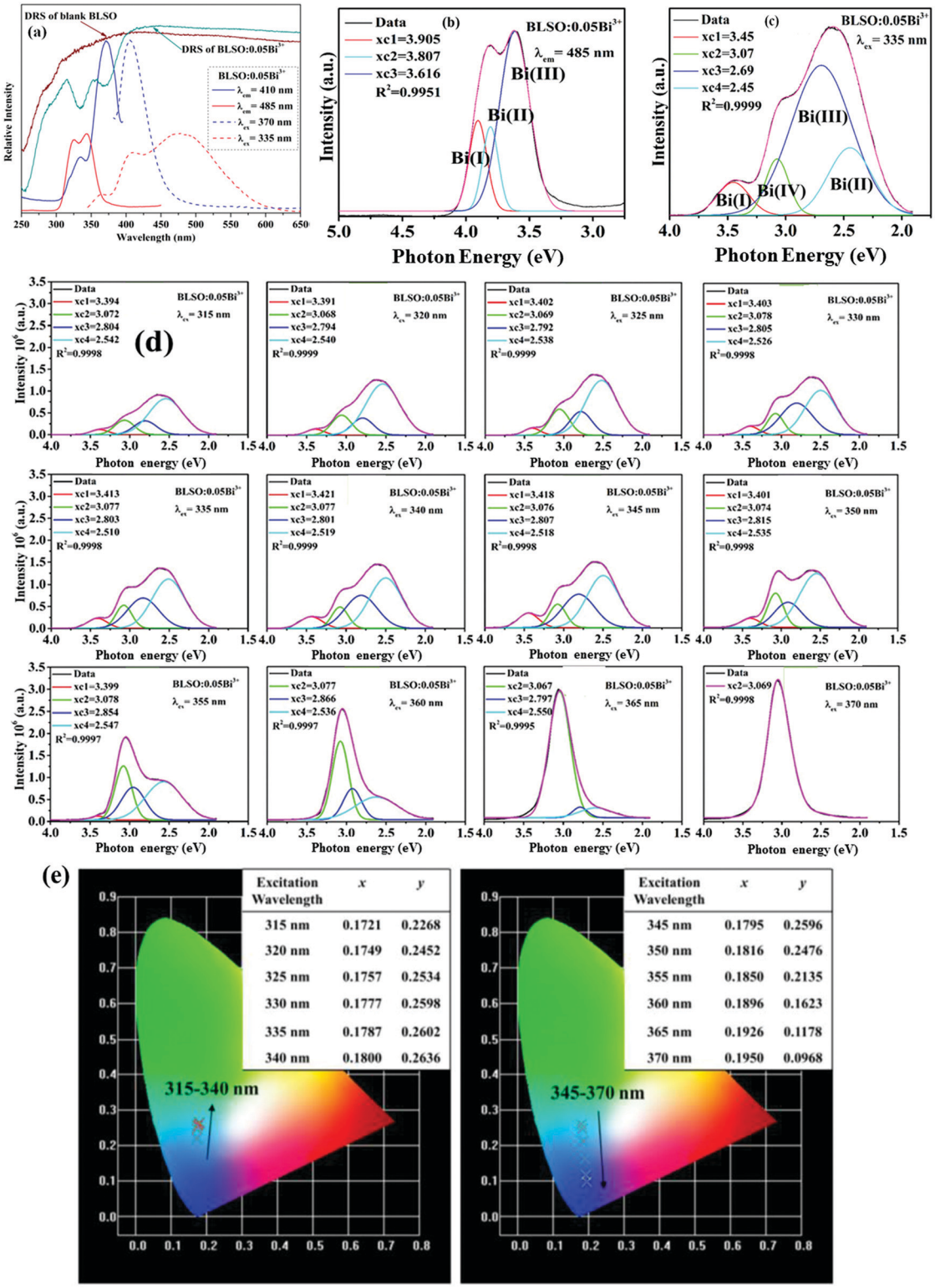

Fig. 7 (a) DRS (diffuse reflectance spectra) of the undoped and Bi^{3+}-doped samples along with the PLE and PL spectra of BLSO:5%Bi^{3+} at various monitored emission and excitation wavelengths, (b and c) the Gaussian deconvolution and fitting of excitation and emission spectra with λ_{em} = 485 nm and λ_{ex} = 335 nm, respectively, (d) Gaussian deconvolution and fitting of the emission spectra at various excitation wavelengths in the range of 315–370 nm, and (e) CIE coordinated diagrams at various excitation wavelengths in the range of 315–370 nm.[110] (Reproduced with permission from ref. 110, copyright 2017 Nature.)

Similarly, the emission spectrum measured under 335 nm UV light excitation (Fig. 7c) was perfectly fitted into four Gaussian bands, having maximum peaks at 3.45 eV (359.4 nm), 3.07 eV (403.9 nm), 2.69 eV (461.0 nm), and 2.45 eV (506.1 nm).

This fitting suggests that the activated Bi^{3+} ions occupy four available crystallographic sites. These four luminescent centers are termed Bi(1), Bi(2), Bi(3), and Bi(4). According to the previous discussions and investigations, it is concluded that the broad-band blue emission, having a maximum at 403.9 nm, is ascribed to the emission of the Bi(4) luminescent center, which is the emission of Bi^{3+} ions occupying the 6-coordinated Lu^{3+} crystallographic sites. The other three emission bands are attributed to the substitution of Bi^{3+} in the other three available Ba^{2+} crystallographic sites.

According to previous studies,[105,111] an efficient energy transfer occurs among the various Ce^{3+}-luminescent centers, which occupy various crystallographic sites. In order to investigate the energy transfer among the four Bi^{3+}-luminescent centers, Gaussian deconvolution and fitting was performed in the measured emission of BLSO:0.05Bi^{3+} phosphor excited over a wide range of excitation wavelengths (315 to 370 nm UV light in increasing steps of 5 nm). The obtained results, plotted in Fig. 7d, reveal various trends as far as the enhancement of the intensity of the Gaussian peaks is concerned. More specifically, the emission spectra over the excitation wavelength range of 315–355 nm show four dominant Gaussian bands, centered at 363.3 nm (3.413 eV), 403.1 nm (3.077 eV), 437.7 nm (2.833 eV), and 494.5 nm (2.518 eV). A further increase of the excitation wavelength to 360, 365, and 370 nm causes changes to the emission spectra and the fitting was achieved by one dominant Gaussian peak, ascribed to the emission of the Bi(4) luminescent center. These results indicate the occurrence of the dominant energy transfer from various luminescent centers, *i.e.* from Bi(1), Bi(2), and Bi(3) to Bi(4).

The widening of the wavelength range of excitation is an index for enhancing the efficient energy transfer to the Bi(4) luminescent centers. This is because of the extensive overlapping of the broad band excitation spectrum with a long tail of Bi(4) with the emission spectrum of Bi^{3+} occupying the three crystallographic sites of Ba^{2+} ions (Fig. 7a). The energy transfer among the Bi(1), Bi(2), and Bi(3) luminescent centers was also observed under excitation in the wavelength range of 315–355 nm. The energy transfer from Bi^{3+}-doped ions in various available crystallographic sites to the co-doped Eu^{3+} ions is discussed in the present work and its explanation is presented in the next section.

The CIE (Commission Internationale de l'Eclairage) chromaticity coordinates of the Bi^{3+}-activated BLSO phosphors at various excitation-wavelengths between 315 and 370 nm UV light in increasing steps of 5 nm were measured. The results, plotted in Fig. 7e, show that the emission color is efficiently tuned from blue (0.1721, 0.2268) to bluish-green (0.1800, 0.2636) upon adjusting the excitation wavelength from 315 nm to 340 nm. Nonetheless, the photoluminescence emission color displays a dramatic variation, changing from bluish green (0.1795, 0.2596) to dark blue (0.1950, 0.0968), as the photoluminescence excitation-wavelength increases from 345 to 370 nm UV light. These results qualify these phosphors with tunable-luminescence as potential materials for use in white LEDs.

3.4 Tb^{3+} occupation in multiple crystallographic sites

Trivalent Tb^{3+}-activated phosphors are broadly used in the development of plasma display panels (PDP) and fluorescent lamps on account of their characteristic highly-efficient narrow-band green emission and the solid vacuum-ultraviolet/ultraviolet (VUV)/(UV) light absorption of the doped Tb^{3+} ions. Most of these narrow-band emitting phosphors are fluorides, with quantum efficiencies higher than 90%, which are low in comparison with the theoretical generation of visible photons (one VUV/UV photon converted to two or more visible photons), whereby a quantum efficiency of up to 200% can be reached as a result of the quantum cutting (QC) phenomenon. Oxides usually exhibit higher quantum efficiency (QE) than fluorides.

Y. Liu[112] and co-workers synthesized a novel $Ba_9Lu_2Si_6O_{24}$:Tb^{3+} (BLSO:Tb^{3+}) oxide phosphor. The BLSO:Tb^{3+} phosphor exhibits efficient green color emission having a dominant peak at 552 nm under 251 nm VUV light excitation with cross-relaxation energy transfer occurring between Tb^{3+} ions. Quantum efficiency, calculated by using direct and indirect methods, showed values of 171% and 144%, respectively, much higher than those of commercially available phosphors that are about 90%. This reveals the high potential of BLSO:Tb^{3+} phosphors for use in PDP and fluorescent lamps. The study of luminescence spectra and decay-time profiles shed light on the cross-relaxation energy transfer.

Photoluminescence excitation measurements were made for the BLSO:2%Tb^{3+} phosphor at monitored wavelengths of 380 and 552 nm. The PLE spectra shown in Fig. 8a display a highly intensive excitation band, having a maximum peak at around 251 nm, along with weak photoluminescence excitation peaks at 282 and 302 nm, at both the monitored emission wavelengths. Weak excitation peaks at longer wavelengths range from 325 to 552 nm (enlarged graph in the inset of Fig. 8a) at the monitored emission wavelength of 552 nm. These excitation bands (251–302) and peaks (325–552) are attributed to the spin-allowed f–d transition and the spin-forbidden f–f transition of Tb^{3+} ions.

The photoluminescence emission spectra of the Tb^{3+}-doped BLSO phosphors at various concentrations of Tb^{3+} ions (x = 0.02, 0.06, 0.1, 0.15, 0.2, 0.4, 0.6, 0.8, 1.0, and 1.2) under 251 nm VUV excitation are depicted in Fig. 8b. Various peaks in the blue to green spectral region are observed. The emission peaks ranging from 350 to 475 nm are attributed to the corresponding emission of the $^5D_3$ to ^7F_J (J = 6, 5, 4, and 3) transition of Tb^{3+} ions. The emission peaks in the range of 475–700 nm are ascribed to the photoluminescence emissions of the $^5D_4$ to ^7F_J transition (where J = 6, 5, 4, 3, 2, 1, and 0) of the activated Tb^{3+} ions.

At a low content (x = 0.02) of the activated trivalent Tb^{3+} in the synthesized BLSO phosphors, the blue emission has a maximum at 380 nm, and due to the $^5D_3$ to ^7F_J transition, the emission spectra have dominant peaks in the blue color region. The blue emission peaks decrease with increasing concentration of Tb^{3+} ions, whereas the emission peaks in the green spectral region become stronger, and the corresponding green emission at 552 nm ($^5D_4$ to $^7F_5$) becomes dominant for x = 0.10.

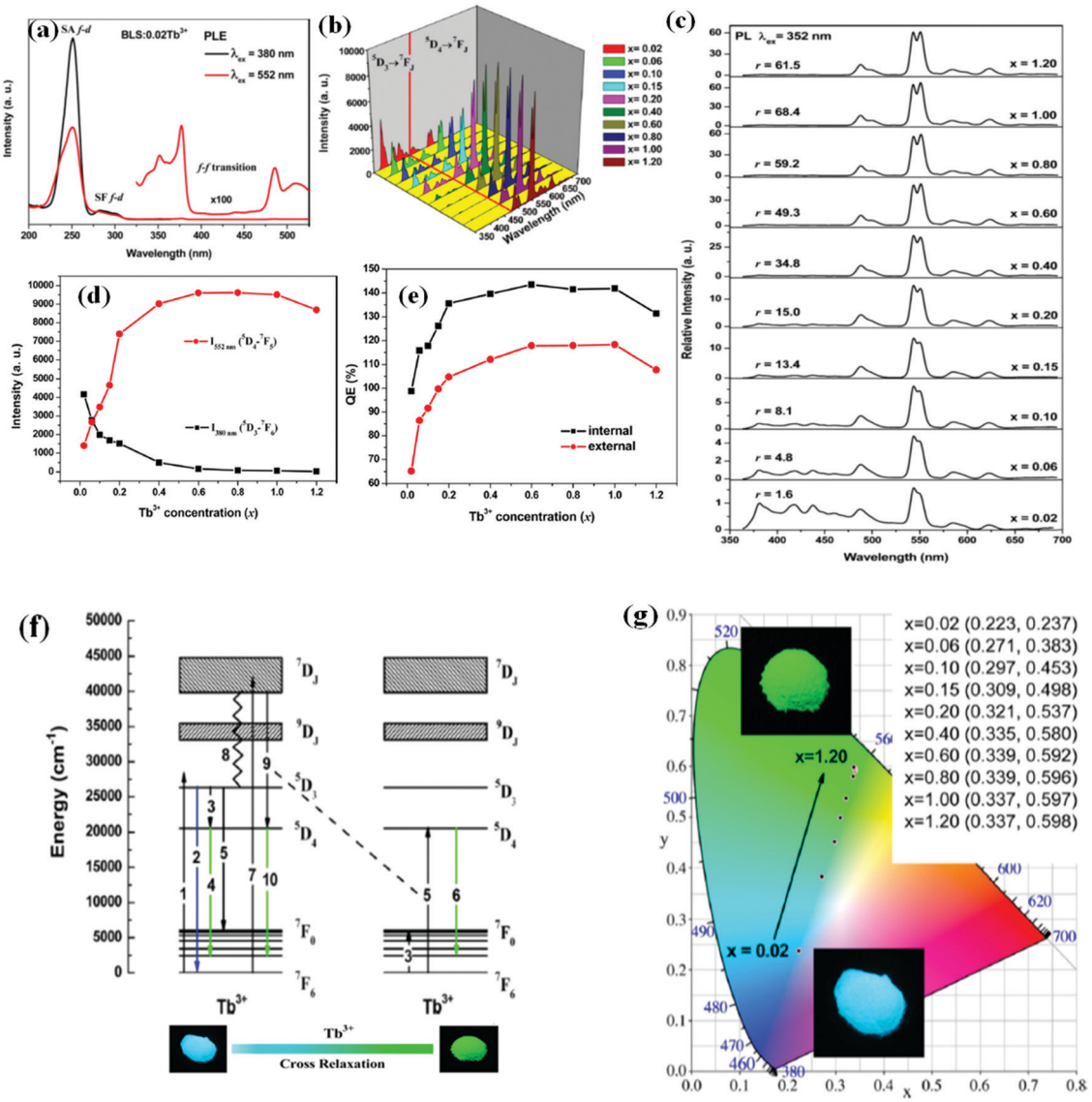

Fig. 8 Features and properties of BLSO:Tb^{3+} phosphors, such as (a) PLE spectra monitored at 380 nm and 552 nm emission wavelengths, PL spectra with various concentrations of Tb^{3+} (x = 0.02–1.20) under (b) 251 nm and (c) 352 nm excitation, (d) emission peak intensities at 380 nm and 552 nm, (e) internal and external quantum efficiencies under 251 nm excitation as functions of Tb^{3+} concentration, (f) mechanisms of cross relaxation, and (g) CIE color coordinate diagram with digital photographs of phosphor samples under 365 nm UV light.[112] (Reproduced with permission from ref. 112, copyright 2016 American Chemical Society.)

At larger Tb^{3+} concentrations ($x > 0.40$), the emission peaks in the blue spectral region nearly disappear, while the green emission peaks remain in the spectra of the Tb^{3+}-doped BLSO phosphors. This behavior is a result of the cross-relaxation energy-transfer process among multiple Tb^{3+} ions. The phenomenon of quantum cutting has been investigated in multiple Tb^{3+}-doped phosphors.[113–122]

Most of these phosphor host lattices have the trivalent Gd^{3+} cation as one of the main constituents. A unique feature is that the emission ratio of $^5D_4$ to $^5D_3$ transition is higher when the 5d energy-level of the doped Tb^{3+} ions is excited, compared with the ratio when the ^6I_J level of the trivalent Gd^{3+} ion becomes excited. The photoluminescence spectra of the BLSO:$x$$Tb^{3+}$ (x = 0.02–1.20) phosphors under 352 nm UV light excitation are shown in Fig. 8c. The emission intensity of $^5D_3$ to $^7F_6$ was kept as a normalized standard. It is clearly observed that the green color emission of $^5D_4$ is dominant for all the Tb^{3+}-dopant concentrations. The results are different from the photoluminescence emission spectra shown in Fig. 8b obtained under 251 nm UV light irradiation, where the blue emission of $^5D_3$ was dominant at the lower Tb^{3+}-dopant concentrations (x = 0.02 and 0.06). It is also observed (Fig. 8c) that the green emission, ascribed to the magnetic dipole transition of $^5D_4$ to $^7F_6$, is split into two emission peaks, having maxima at 544 nm and 552 nm, owing to the Stark splitting of the doping Tb^{3+} ions.

The peak intensity of the green color emission around 552 nm is the dominant emission peak at all the concentrations of Tb^{3+} ions under excitation with 251 nm VUV light. On the

other hand, under 352 nm UV light excitation, the green emission peak has a maximum at 544 nm at lower contents of Tb^{3+} (x = 0.02–0.40) ions. The maximum position shifts to 552 nm at higher concentrations (x = 0.60–1.20) of Tb^{3+} ions. The value of r, shown in Fig. 8c, illustrates the ratio of the highest photoluminescence peak intensity (544 or 552 nm) to that of the standard emission peak intensity at 380 nm. It is clearly shown that the value of r increases upon increasing the concentration of the Tb^{3+} ions from x = 0.02 to 1.00, but it is reduced for x = 1.20.

A similar trend is further observed in the enhancement of the intensity of the $^5D_3$–$^7F_6$ transition (Fig. 8d) and in the quantum efficiency upon increasing the concentration of the Tb^{3+} dopant (Fig. 8e). The value of r is greatly increased upon increasing the concentration of the Tb^{3+} dopant under 352 nm excitation. The enhancement of the value of r should be assigned to the cross-relaxation energy transfer occurring among the Tb^{3+} dopants in the BLSO phosphor host lattice through $^5D_3$ to $^5D_4$ and $^7F_6$ to $^7F_0$ transitions.

The energy levels of the Tb^{3+} ions in the BLSO phosphor matrix plotted in Fig. 8f elucidate the cross-relaxation of the energy-transfer phenomenon. More specifically, when an electron is excited into an excited state of the $^5D_3$ energy level (process 1), blue emission of $^5D_3$ occurs (process 2), as a result of multi-photon relaxation. The cross-relaxation can also populate the $^5D_4$ energy state (process 3). The energy gap between $^5D_3$ and $^5D_4$ is $\sim$5800 cm^{-1}, which is similar to the difference between $^7F_0$ and $^7F_6$ ($\sim$6000 cm^{-1}) in the Tb^{3+}-doped BLSO phosphors, resulting in the green emission of $^5D_4$ (process 4).

When the two Tb^{3+} dopants are close together, a resonance condition will occur, in which the transfer of an electron from the $^5D_3$ to $^5D_4$ energy state is balanced by the promotion of an electron from the $^7F_6$ to $^7F_0$ energy state (process 3). The excited electron to the $^7F_0$ energy level can then move to the ground energy level *via* the non-radiative process. The energy difference between $^5D_3$ and $^7F_0$ is $\sim$20 300 cm^{-1}, which is very close to $\sim$20 500 cm^{-1} of the energy difference between the $^5D_4$ and $^7F_6$ energy states. Accordingly, another cross-relaxation (process 5) can also occur at the higher concentration of Tb^{3+} ions, which brings the Tb^{3+} ions close enough in the BLSO-phosphor host lattice. Consequently, further efficient green emission of $^5D_4$ is obtained (process 6).

When the Tb^{3+} concentration is further increased, the distance between the Tb^{3+} dopants becomes smaller. This facilitates the occurrence of resonance energy transfer through cross-relaxation. A close observation of the emission intensity ratios in Fig. 8c supports the influence of the enhancement of cross-relaxation on the photoluminescence characteristics of the BLSO:Tb^{3+} phosphors, and manifests the enhancement of the efficiency of resonance energy-transfer with $^5D_3$ excitation.

The photoluminescence quenching at higher concentrations of the Tb^{3+} dopant in BLSO phosphors is attributed to the interactions of cross-relaxation of energy transfer. The electrons are excited to the ^7D_J energy state (process 7) under 251 nm light excitation. Some of these excited electrons are relaxed to the $^5D_3$ energy level by the relaxation of the multiphoton process (process 8) and are further moved to follow processes 2 to 6, leading to blue and green color emission. The energy separation between the lowest ^7D_J energy level and $^5D_4$ is $\sim$19 300 cm^{-1}, which is close to $\sim$20 500 cm^{-1} of the energy difference between the $^5D_4$ and $^7F_6$ energy levels. Therefore, when the excited electrons move from the ^7D_J energy level to $^5D_4$ energy level, the electrons in the $^7F_6$ ground energy state are also excited to the $^5D_4$ energy state by resonance energy transfer, following the path of processes 9 to 5, provided that the doped trivalent Tb^{3+} ions are close enough to one another. Furthermore, when the cross-relaxation as shown in processes 9 to 5 takes place, one electron of the ^7D_J energy state produces two excited electrons in the $^5D_4$ energy state, which generates two green-emitting photons, on account of processes 6 and 10.

These phenomena enhance the quantum efficiency of the Tb^{3+}-doped phosphors to 100% or even more, enabling 200% enhancement. The cross-relaxation energy-transfer process which results in quantum cutting in the trivalent Tb^{3+}-doped BLSO phosphors is not on the basis of transitions that occurred from ^7D_J to $^5D_{1,2,3}$ and $^7F_6$ to $^5D_4$, but it is due to ^7D_J to $^5D_4$ and $^7F_6$ to $^5D_4$ transitions. Similar phenomena have also been realized in Tb^{3+}/Gd^{3+}-activated $CsCdBr_3$ crystals; however, these transitions are very rare in these systems.[123]

It has been observed that the BLSO phosphors with various Tb^{3+}-dopant concentrations display tunable color emission from light blue to efficient green. The tunable color emission is depicted in the CIE chromaticity coordinate diagram in Fig. 8g. The digital photographs show the tuning of the coordinates from (0.223, 0.237) for 0.02 Tb^{3+} content to (0.337, 0.598) at a higher concentration of Tb^{3+} ions (x = 1.20).

4. Photoluminescence tuning *via* energy transfer in BLSO phosphors

The transfer of energy among various dopants is the most powerful and efficient strategy for broadening the luminescence spectrum of single-phase phosphors in order to cover the whole visible spectral region. This section reports on characteristic and promising cases of both double and triple doping in BLSO phosphors.

4.1 Double doping in the BLSO phosphor host

4.1.1 Eu^{2+}–Mn^{2+}. As discussed above, a single activator can occupy various crystallographic sites of BLSO phosphors, enabling tunable emission of different colors. The achievement of broadband adjustable and tunable emission, deriving from various energy-transfer processes which are facilitated by various co-dopant activators, reveals the potential of inorganic materials for use in various applications, like solid-state lighting, erasable optical data storage, and temperature sensors.[124–127]

Among several rare-earth and transition-metal dopants, the efficient Eu^{2+}–Mn^{2+} combination is very popular. The divalent Mn^{2+} dopant is a transition metal that exhibits various color emissions, such as green and red emissions, ascribed to the Mn^{2+} occupation in the tetrahedron and in the octahedron-field

environment, respectively. The photoluminescence excitation spectra of the divalent Mn^{2+} dopant are often located in the blue and green spectral regions.[128–130] Hence, the photoluminescence spectra of the divalent Mn^{2+} ions mostly overlap with the blue or green emission of the divalent Eu^{2+} activators. The energy transfer from Eu^{2+} to Mn^{2+} leads to tunable broadband emission in a single-phase phosphor.

Our previous work[38] reports on the development of Eu^{2+}/Mn^{2+}-*co*-doped $Ca_xBa_{9-x}Lu_2Si_6O_{24}$ (CBLSO) single composition phosphors with white light emission, developed by a conventional solid-state reaction route. The addition of Mn^{2+} ions as a co-dopant resulted in red color emission with a dominant peak at around 618 nm, through efficient energy transfer from the divalent Eu^{2+} (sensitizer) to divalent Mn^{2+} (activator) ions following a dipole–dipole interaction. More interestingly, the substitution of the Ca^{2+} and Mn^{2+} ions also leads to improvement in the thermal stability of the CBLSO phosphors. These properties qualify the synthesized $Ca_xBa_{(9-x)}Lu_2Si_6O_{24}$:$Eu^{2+}$/$Mn^{2+}$ phosphors as promising candidates for single-phase ultraviolet excitable white-light-emitting phosphors.

The influence of the concentration of Mn^{2+}, as a co-dopant, on various characteristics of CBLSO was also investigated. The photoluminescence emission spectra of $Ca_{1.5}Ba_{7.38-y}Lu_2Si_6O_{24}$:$0.12Eu^{2+}/yMn^{2+}$ single-phase phosphors (for y = 0–1) under 343 nm excitation are shown in Fig. 9a. These spectra show that doping with divalent Eu^{2+} and Mn^{2+} as a co-dopant in the produced CBLSO phosphor host can produce tunable white light, since a broad band spectrum with the bands of

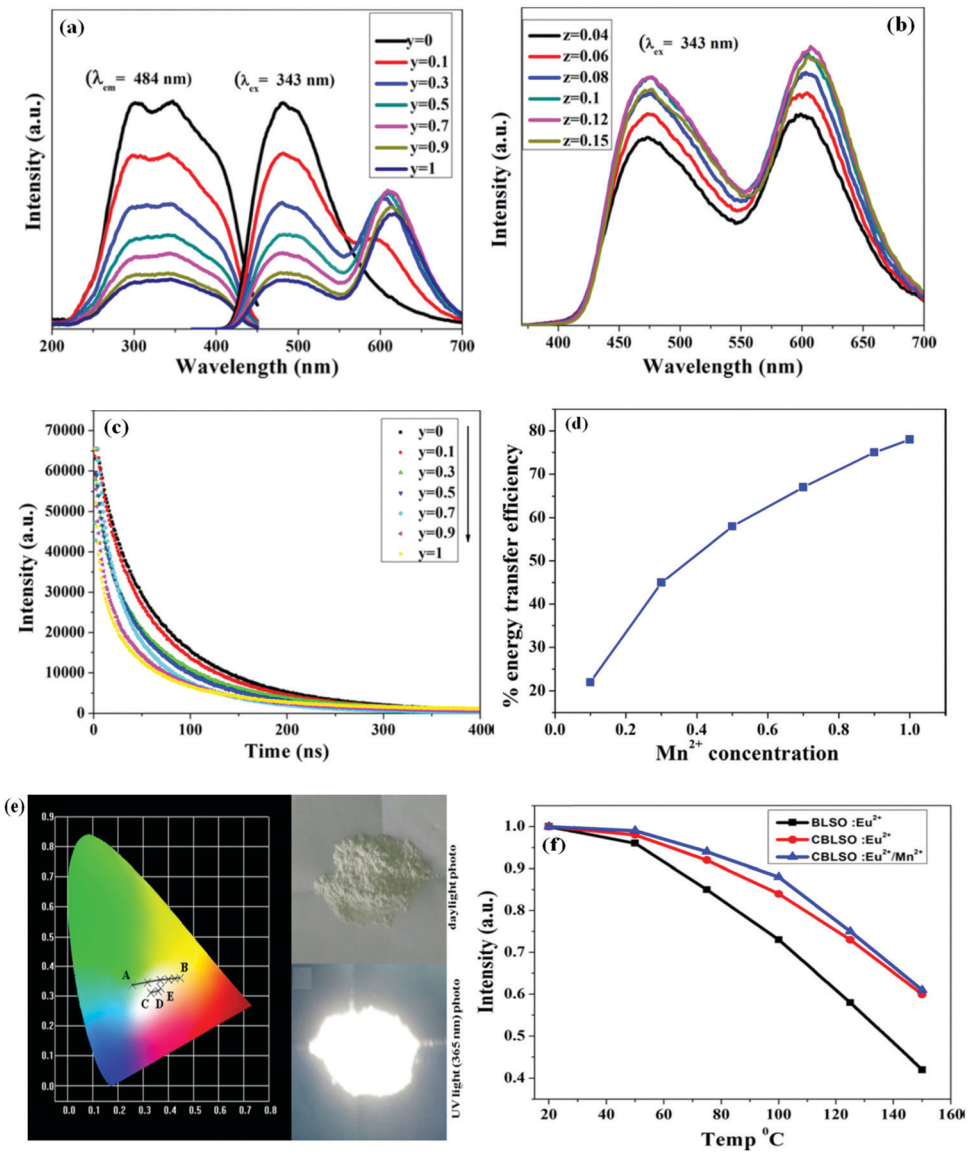

Fig. 9 (a) PLE and PL spectra of CBLSO:$0.12Eu^{2+}/yMn^{2+}$ (y = 0, 0.1, 0.3, 0.5, 0.7, 0.9, and 1) at λ_{ex} = 343 nm and λ_{em} = 484 nm, (b) PL spectra of CBLSO:$0.3Mn^{2+}/zEu^{2+}$ (z = 0.04–0.15), (c) fluorescence decay-time profiles of CBLSO:$0.12Eu^{2+}/yMn^{2+}$ (y = 0, 0.1, 0.3, 0.5, 0.7, 0.9, and 1) at λ_{ex} = 343 nm and λ_{em} = 484 nm, (d) energy-transfer efficiency, (e) CIE chromaticity diagram with digital photographs under ordinary light and 365 nm UV light, and (f) thermal stability of BLSO:Eu^{2+}, CBLSO:Eu^{2+}, and CBLSO:Eu^{2+}/Mn^{2+} phosphors.[38] (Reproduced with permission from ref. 38, copyright 2017, American Chemical Society.)

blue-greenish and red-emission, peaking at 484 and 500 nm (due to the $4f^6 5d^1$–$4f^7$ transitions of the doped Eu^{2+} ions), and also at 618 nm (as a result of the $^4T_1(^4G)$–$^6A^1(^6S)$ transitions of the divalent Mn^{2+} ions), was observed. The broad and symmetric-emission bands of $Ca_{1.5}Ba_{7.5}Lu_2Si_6O_{24}$:$Eu^{2+}$/$Mn^{2+}$ are attributed to the transitions of Eu^{2+} and Mn^{2+} occupying the three crystallographically distinct Ba^{2+} sites in the host structure. The photoluminescence intensity of Eu^{2+} decreases with the increase of Mn^{2+} content (y), and the intensity of the red color emission attributed to Mn^{2+} increases with the increase of Mn^{2+} concentration (y) up to the appearance of concentration quenching at Mn^{2+} content y = 0.7, which witnesses the energy transfer from Eu^{2+} to Mn^{2+} ions.

The photoluminescence emission spectra of CBLSO phosphor samples for fixed Mn^{2+} concentration (y = 0.3) and for various Eu^{2+} concentrations (z = 0.04, 0.08, 0.1, 0.12, and 0.15) are plotted in Fig. 9b. The intensity of the red emission of Mn^{2+} in CBLSO is increased with the increase of Eu^{2+} concentration up to z = 0.12. A further increase in Eu^{2+} concentration results in a decrease in the emission intensity, ascribed to concentration quenching. The increase in PL emission of Mn^{2+} with increasing content of Eu^{2+} by keeping the Mn^{2+} content at a fixed value also confirms the effective energy transfer from the Eu^{2+} (sensitizer) to Mn^{2+} (activator) in the CBLSO phosphor host.

The above results validate that transfer of energy from the divalent Eu^{2+} to Mn^{2+} co-dopants efficiently occurs. The measurement of decay time profiles is a parameter of great importance since it can effectively validate this hypothesis. The photoluminescence decay-time curves of the synthesized CBLSO:0.12Eu^{2+}/yMn^{2+} were measured under 343 nm UV light excitation at 484 nm monitored emission wavelength. The results were fitted well to the sum of the following second order exponential decay time components:

$$I(t) = A_1 \exp(-t/\tau_1) + A_2 \exp(-t/\tau_2), \quad (2)$$

where τ_1 and τ_2 are the decay-time constants, while A_1 and A_2 are the exponential constants. Therefore, the average photoluminescence decay times (τ^*) can be found by the formula[38]

$$\tau^* = \frac{A_1\tau_1^2 + A_2\tau_2^2}{A_1\tau_1 + A_2\tau_2}. \quad (3)$$

The results obtained for the average photoluminescence decay time (τ^*), measured using the above eqn (3), are exhibited in Fig. 9c. The photoluminescence decay time shows a decreasing trend from 161 to 133, 105, 93, 70, 68, and 64 ns for the increase of y = 0–1, respectively. The decrease of the photoluminescence decay time with increasing Mn^{2+} concentration validates the existence of efficient energy transfer from the divalent Eu^{2+} (sensitizer) to Mn^{2+} (activator) ions in the Eu^{2+}/Mn^{2+} co-doped CBLSO phosphors.

To further understand the transfer of energy from Eu^{2+} to Mn^{2+} ions, the energy transfer efficiency (η) for various Mn^{2+} concentrations was calculated by eqn (4):

$$\eta = 1 - I_s/I_{s0} \quad (4)$$

where I_s and I_{s0} are the luminescence intensities in the presence and absence of the activator Mn^{2+}, respectively. The energy transfer efficiency (η) of the activated divalent Eu^{2+} (sensitizer) ions to the co-doped Mn^{2+} (activator) as a function of Mn^{2+} content is shown in Fig. 9d. The efficiency of energy transfer is increased with the increase of Mn^{2+} concentration and reaches 67% for the optimized concentration of the Mn^{2+} (y = 0.7) co-dopant.

The color-coordinate tuning of CBLSO:0.2Eu^{2+}/yMn^{2+} co-doped phosphors (where y = 0–1) under UV light (343 nm) excitation is depicted in Fig. 9e. The emission color is tuned from blue-greenish (wide-band) to white and yellow (*i.e.* from point A to B respectively). The emission-color points, including the white-light points (*i.e.* the points named C, D, and E), are also seen in this diagram. Accordingly, a controllable emission color can be achieved by adjusting the Mn^{2+} content. This qualifies the produced color-tunable CBLSO:Eu^{2+}/Mn^{2+} phosphors as efficient candidates for single-phase white-light-emitting diodes, where the tuning ability can be easily achieved by simply adjusting the content of the Ca^{2+} and Eu^{2+}/Mn^{2+} constituents. The photographic images of these phosphors are shown on the right side of Fig. 9e. The produced CBLSO:Eu^{2+}/Mn^{2+} phosphor sample is colorless under ordinary daylight, but it emits white light with high brightness under 365 nm UV light excitation.

The influence of temperature on the emission spectra of $Ca_xBa_{(9-x)}Lu_2Si_6O_{24}$:$Eu^{2+}$/$Mn^{2+}$ phosphors under 343 nm excitation for the samples with x = 0 and 1.5 is plotted in Fig. 9f. The comparison of these two samples (x = 0 and x = 1.5) along with the red emission of the Mn^{2+} co-doped CBLSO phosphor shows that the stability against increasing temperature is increased by increasing the Ca^{2+} content in the CBLSO:0.2Eu^{2+} phosphor host lattice. The excellent improvement of thermal stability can be mainly attributed to two reasons. One reason is related to the contraction produced in the unit volume. As a result of this, the interactions between the doped Eu^{2+} and O^{2-} (which are crystal-field effects and the nephelauxetic effect in the 5d orbital of Eu^{2+}) vary. The other reason is linked to the fact that the activator Eu^{2+} is moved from the Ba(1) site to the Ba(2) and Ba(3) sites when the content of Ca^{2+} ions is increased. This, consequently, creates various surrounding environments for the activated Eu^{2+} ions.

4.1.2 Ce^{3+}–Mn^{2+}. In the literature, there are reports on the orange-red emission of Mn^{2+}-doped phosphors. However, the d–d absorption transitions for this ion are difficult to pump (*i.e.* to excite this transition) due to the nature of the strongly forbidden transitions. Interestingly, the trivalent Ce^{3+} dopants have a spin-allowed transition among the 5d and 4f energy levels. Hence, efficient broadband luminescence is obtained owing to the spin allowed 4f–5d electric-dipole transition. Therefore, trivalent Ce^{3+} dopants are often used in activator/sensitizer phosphor systems with divalent Mn^{2+} ions used as co-dopants.

The team of K. Song[111] developed new highly-efficient tunable bluish-cyan to red-emitting BLSO phosphors co-doped with Ce^{3+} and Mn^{2+} activators, where efficient energy transfer occurs from the trivalent Ce^{3+} to Mn^{2+} ions.

More interestingly, the efficiency of energy transfer was further intensified with self-charge compensation, due to the occupation of the available crystallographic cation sites by Ce^{3+} activators. This led to highly stable red emission peaking at 610 nm, and a high internal-quantum efficiency of 70%, with 84% of the quantum efficiency remaining at 160 °C.

The photoluminescence excitation and emission spectra of Ce^{3+} occupying various crystallographic sites and Mn^{2+} single-doped phosphors are shown in Fig. 10a. The bluish-cyan emission is a result of the Ce^{3+} occupying the three crystallographic sites of Ba^{2+}, whose spectrum overlaps the excitation spectrum of the divalent Mn^{2+} dopant. The overlapping of the emission of the sensitizer with the excitation of the activator is necessary for an efficient energy transfer.

A series of the photoluminescence spectra of BLSO phosphors co-doped with Ce^{3+} and Mn^{2+} activators are presented in Fig. 10b. Strong red emission at around 610 nm is observed in the spectra of BLSO:10%Ce^{3+}/$x$$Mn^{2+}$ (x = 0.00–0.20) co-doped phosphors. The intensity of this red-color emission is increased by increasing the content of the Mn^{2+} ions and reaches a maximum for x = 0.15. A further increase of Mn^{2+} concentration ($Mn^{2+} > 0.15$) causes a decrease in the intensity of the red-color emission, ascribed to concentration quenching.

An interesting and unusual phenomenon was the enhancement of the bluish-cyan emission of Ce^{3+} occurring with increasing concentration of Mn^{2+} dopant ions. This is ascribed to the occupation by the activators on account of self-charge compensation. As mentioned above, the trivalent Ce^{3+} ions can occupy both the divalent Ba^{2+} and trivalent Lu^{3+} crystallographic sites. Although the Ce^{3+} activator is smaller than the Ba^{2+} cation, in Ce^{3+} singly-doped BLSO phosphors, the occupation of the site of the divalent Ba^{2+} cation by the trivalent Ce^{3+} cation can be restricted by the charge difference between Ce^{3+} and Ba^{2+}. Nonetheless, when the divalent Mn^{2+} is co-doped into the BLSO host lattice, the charge difference can be compensated for by the replacement of the divalent Mn^{2+} in the trivalent Lu^{3+} site. The inset of Fig. 10b shows the photoluminescence excitation spectrum of the optimized BLSO:10%Ce^{3+}/15%Mn^{2+} phosphor, monitored at 610 nm emission wavelength. The broadband photoluminescence excitation spectrum, having a maximum at 333 nm, is similar to the photoluminescence excitation spectrum of Ce^{3+} occupying divalent Ba^{2+}-crystallographic sites in the Ce^{3+}-doped BLSO phosphors.

The efficiency of energy transfer from the trivalent Ce^{3+} to divalent Mn^{2+} activator is confirmed further by the fluorescence decay-time profiles of the emission of the trivalent Ce^{3+}-dopant. The decay-time curves plotted in Fig. 10c reveal that the decay becomes faster with increasing concentration of the divalent Mn^{2+} co-doped ions. The luminescence decay time (τ) was recorded by integrating the normalized photoluminescence decay profiles. The decay time (measured for the emission of Ce^{3+}) in BLSO:10%Ce^{3+},$x$$Mn^{2+}$ phosphors decreases from 26 ns

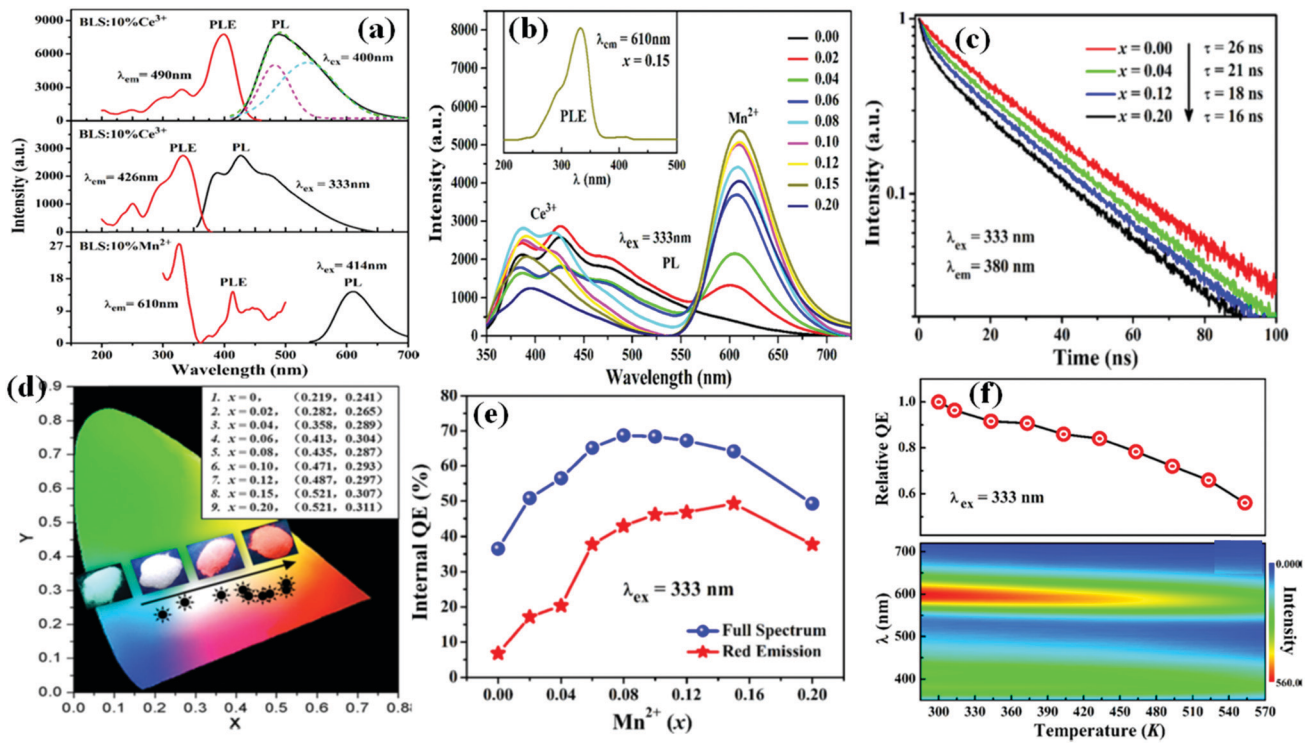

Fig. 10 (a) PLE and PL spectra of BLSO phosphors with 10%Ce^{3+} excited at 333 nm, at 400 nm, and with 10%Mn^{2+}, (b) PL spectra with 10%Ce^{3+}/$x$$Mn^{2+}$ (x = 0.00–0.2) co-doping along with the PLE spectrum in the inset, (c) fluorescence decay-time profiles for 10%Ce^{3+}/$x$$Mn^{2+}$ (x = 0.00–0.2) co-doping at 333 nm excitation and 380 nm monitored emission wavelengths, (d) CIE color coordinate tuning with digital photographs under 365 nm UV light, (e) internal-quantum efficiency for 10%Ce^{3+}/$x$$Mn^{2+}$ (x = 0.00–0.2) co-doping, and (f) diagrams for evaluating thermal stability.[111] (Reproduced with permission from ref. 111, copyright 2015 American Chemical Society.)

to 21, 18, and 16 ns with $x = 0$, 0.04, 0.12, and 0.20, respectively. This decrease supports the occurrence of the transfer of energy from Ce^{3+} to Mn^{2+} in the BLSO phosphor host.

The efficient emission-color tuning, from cyan to red, by co-doping with divalent Mn^{2+} ions is depicted in the CIE chromaticity coordinate diagram in Fig. 10d. The efficient emission-color tuning under a 365 nm UV emitting lamp by co-doping with various concentrations of Mn^{2+} ions in the co-doped BLSO:Ce^{3+} phosphors is also shown in the digital photographs in the inset of Fig. 10d. The internal-quantum efficiency and the thermal stability of the activated Ce^{3+}/Mn^{2+} co-doped BLSO phosphors are shown in Fig. 10e and 10f, respectively.

4.1.3 Bi^{3+}–Eu^{3+}. The trivalent Bi^{3+} dopant acts as an effective sensitizer for activating the trivalent Eu^{3+} ion in the multiple-phosphor host lattice.[131,132] The team of Y. Guo[110] investigated the multi-centered photoluminescence characteristics and the crystal-site engineering of Bi^{3+}/Eu^{3+}-*co*-doped $Ba_9Lu_2Si_6O_{24}$ single-phase phosphors in order to obtain efficient and tunable white light. Due to the complex mechanism of the energy transfer, the tuning of the multi-centered photoluminescence was attained by efficiently adjusting the photoluminescence excitation-wavelength or by controlling the concentration of the rare-earth ions.

The photoluminescence emission spectra of BLSO:0.07Bi^{3+}/$y$$Eu^{3+}$ (y = 0.0025–0.025) co-doped phosphors were recorded under 344 and 370 nm excitation, see Fig. 11a and b, respectively. The intensity owing to the Bi^{3+} ions is decreased and the intensity of the red-emission peak, ascribed to the co-activated Eu^{3+} ions, is increased with the increase of the concentration of Eu^{3+} ions. However, no concentration quenching on account of Eu^{3+} was observed in the range of y = 0.0025–0.0250, which confirms the existence of efficient energy transfer from Bi^{3+} to Eu^{3+} ions in the BLSO phosphor host lattice.

The characteristic CIE chromaticity coordinate diagrams of the BLSO:0.07Bi^{3+}/$y$$Eu^{3+}$ (y = 0.0025–0.0250) phosphors are presented in the insets of Fig. 11a and b for the two excitation wavelengths. The position of the color coordinates (x, y) shifts from bluish-green to pink across the entire visible white-light region under 344 nm and 370 nm UV light excitation, respectively.

The photoluminescence excitation spectra monitored at 611 nm emission wavelength of the Bi^{3+}/$y$$Eu^{3+}$ (for 0.07Bi^{3+} and y = 0.0025–0.025) co-doped BLSO phosphors are depicted in Fig. 11c. The photoluminescence excitation shows a broadband ranging from 200 to 500 nm. The 200–280 nm range and the small peak at 464 nm are attributed to the charge-transfer band (CTB) of Eu^{3+}–O_2 and to the $^7F_0$ to $^5D_2$ transition of the Eu^{3+} ions. The broadband from 300–400 nm is associated with the trivalent Bi^{3+} ions. The inset of Fig. 11c shows the fitting of the photoluminescence excitation to four deconvoluted Gaussian peaks. This supports that four kinds of Bi^{3+} luminescent centers contribute to the red emission of the trivalent Eu^{3+} ions.

In order to shed more light on the contribution of the different Bi^{3+} centers to the luminescence of Eu^{3+}, the emission spectra of the optimized BLSO:0.07Bi^{3+}/0.0075Eu^{3+} phosphor were measured under excitation in the range of 330–370 nm (UV light) in steps of 5 nm (Fig. 11d). Their corresponding chromaticity coordinate diagram is shown in Fig. 11e. A variety of color emissions, due to Bi^{3+} and Eu^{3+}, as well as of intensities was recorded. The emission color was efficiently tuned from white to reddish-purple upon increasing the photoluminescence excitation wavelength from 330 to 370 nm. Thus, the emission color can efficiently be tuned by adjusting the concentration of Eu^{3+} and the excitation wavelength.

The energy-transfer mechanism and the generation of tunable and efficient white light are related to the luminescence characteristics of Bi^{3+} and Eu^{3+} in the co-doped BSLO phosphors under UV light irradiation. Indeed, under 344 nm UV light excitation, the three luminescent centers Bi(I), Bi(II), and Bi(III) are excited, resulting in broadband blue/green emission (Fig. 11f). The efficient energy transfer from these three Bi^{3+} luminescent centers to Eu^{3+} ions also results in generating warm white light. Under 370 nm UV light irradiation, the energy is trapped in the Bi(IV) luminescent center, leading to strong blue emission, which further transfers its energy to the co-doped Eu^{3+} ions, and, as a result, tunable photoluminescence emission from blue to the red spectral region is attained (Fig. 11g).

The thermal stability of phosphors is of great importance as far as their potential application in white LEDs is concerned. The stability against the temperature of the optimized BLSO:0.07Bi^{3+}/0.0075Eu^{3+} phosphor under 344 and 370 nm excitation was recorded over a wide temperature range of 299–503 K (Fig. 11h and i, respectively). The intensity in both cases decreases with increasing temperature. The remaining intensity at 423 K (150 °C) was 66.1% and 72.8% (under 344 and 370 nm excitation, respectively) of the value recorded at room temperature.

4.2 Triple doping in BLSO phosphors

Compared with double doping in activated BLSO phosphors, the triple doping originating from different emission centers and their efficient energy transfer provides more opportunities for photoluminescence tuning. In the following sections, two interesting cases are reported.

4.2.1 Ce^{3+}–Mn^{2+}–Tb^{3+}. Doping with divalent Mn^{2+} and trivalent Tb^{3+} ions in various phosphor-host lattices leads to characteristic color emission in the red and green spectral regions, ascribed to the d–d and f–f transitions, respectively.[133,134] However, the d–d and f–f absorption transitions of these activators are crucial to excite over a wide range of UV light. Dopants such as Eu^{2+} and Ce^{3+}, having a 5d–4f spin-allowed transition, are used as sensitizers to be co-doped with Mn^{2+}/Tb^{3+}, whereby they efficiently transfer some of their energy to activate Mn^{2+} and Tb^{3+} ions in order to emit their characteristic color. Our previous work[61] reports on the successful development of novel full color-emitting BLSO:$Ce^{3+}/Mn^{2+}/Tb^{3+}$ single-phase phosphors by using a high-temperature solid-state reaction route.

The influence of the divalent Mn^{2+} content on the photoluminescence excitation (PLE) and emission (PL) spectra of the Ce^{3+}/Mn^{2+} co-doped BLSO phosphors is shown in Fig. 12a. The enhancement of Mn^{2+} concentration (*i.e.* the decrease of

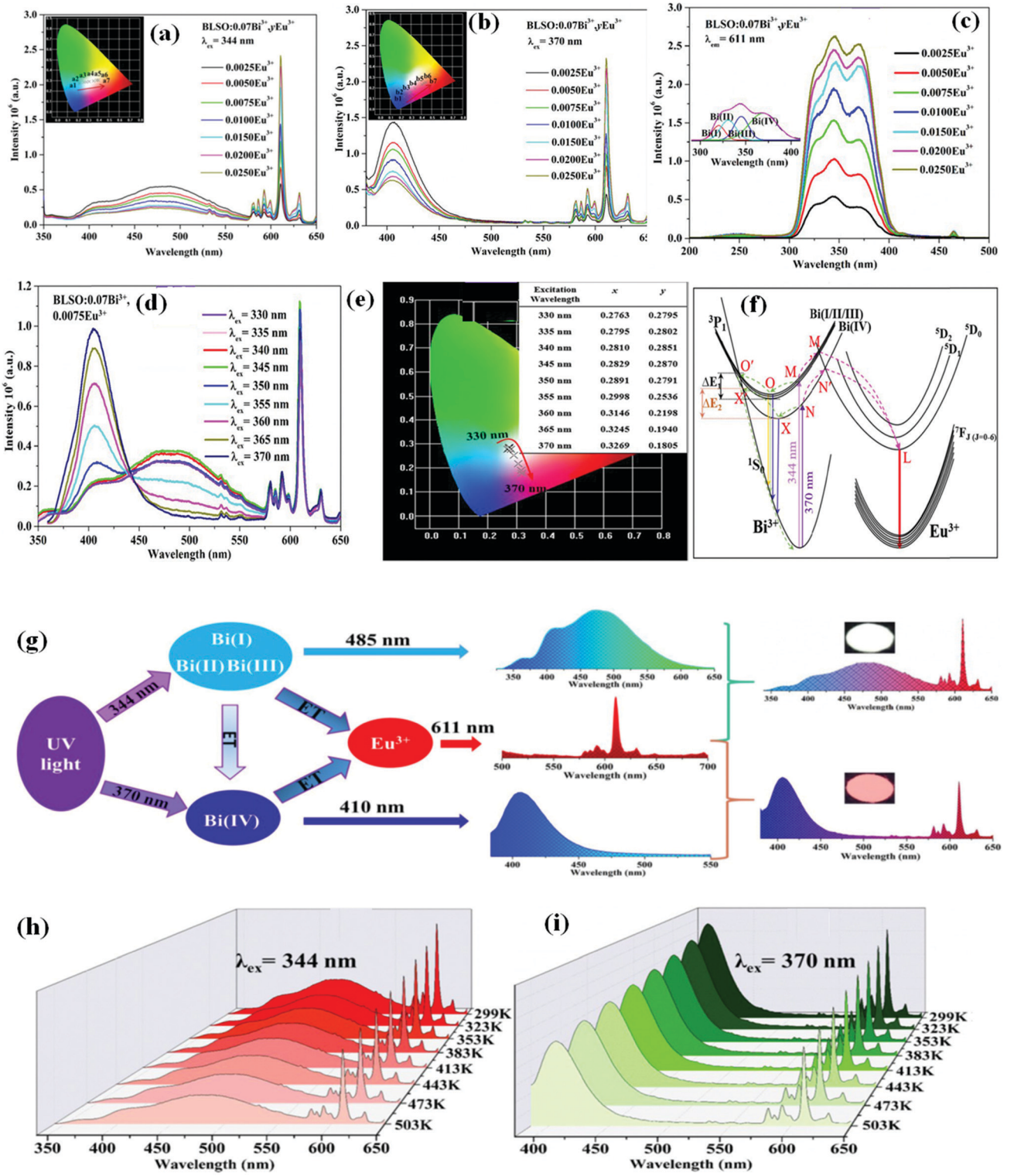

Fig. 11 Photoluminescence emission spectra (along with their corresponding CIE chromaticity coordinate diagrams in the insets) of BLSO:7%Bi^{3+}/yEu^{3+} (y = 0.0025–0.025) phosphors under (a) 344 nm and (b) 370 nm excitation, (c) photoluminescence excitation spectra monitored at 611 nm emission wavelength (along with a Gaussian fitting of an excitation spectrum in the inset), (d) emission spectra and (e) CIE chromaticity coordinate tuning of the optimized BLSO:0.07Bi^{3+}/0.0075Eu^{3+} phosphor under excitation in the range of 330–370 nm, (f) the configurational coordinate diagram of the ground and excited states of Bi^{3+} and Eu^{3+} activators, (g) schematic representation of the energy-transfer mechanism for generating tunable white light, and the temperature dependence of the PL spectra of the optimized phosphor under excitation at (h) 344 nm and (i) 370 nm.[110] (Reproduced with permission from ref. 110, copyright 2017 Nature.)

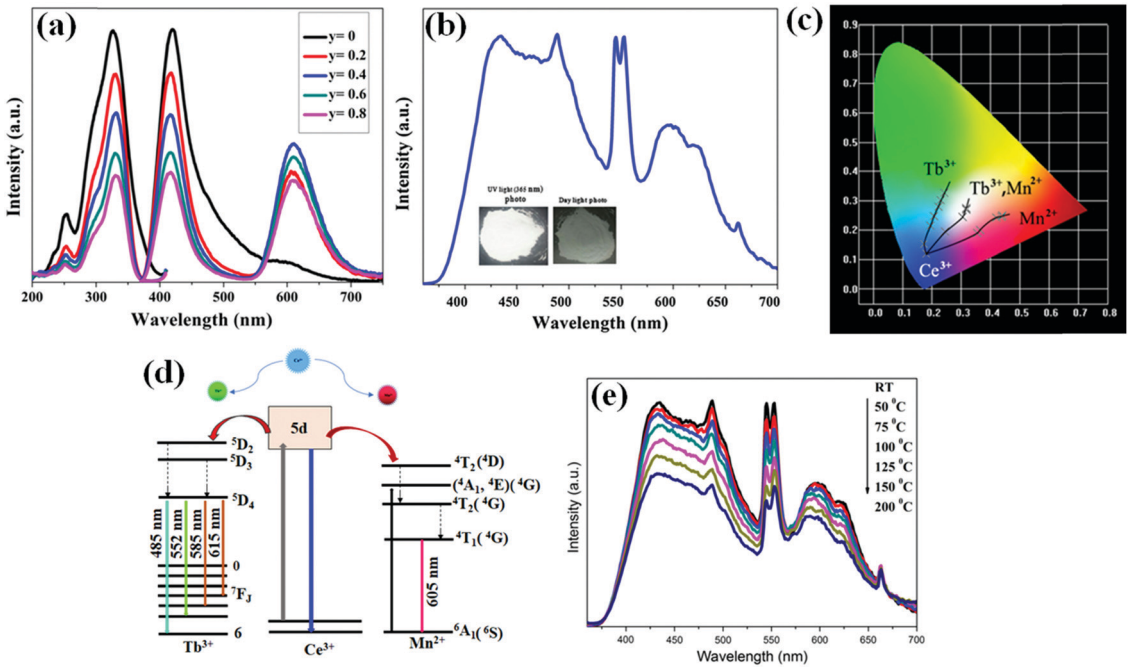

Fig. 12 (a) PLE and PL spectra of BLSO:9%Ce^{3+}/yMn^{2+} (y = 0–0.8) phosphors at λ_{ex} = 332 nm and λ_{em} = 424 nm, (b) emission spectrum of the optimized BLSO:9%Ce^{3+}/20%Mn^{2+}/8%Tb^{3+} phosphor under 345 nm excitation and digital photographs under ordinary daylight and 365 nm UV, (c) CIE color coordinate tuning for Ce^{3+}/Mn^{2+}/Tb^{3+} tri-activated BLSO phosphors under 345 nm UV light excitation, (d) schematic representation of energy transfer, and (e) temperature-dependent emission spectra for the optimized BLSO:9%Ce^{3+}/20%Mn^{2+}/8%Tb^{3+} phosphor under 345 nm UV light irradiation.[61] (Reproduced with permission from ref. 61, copyright 2017 Springer.)

the Ce^{3+}/Mn^{2+} ratio) causes a decrease of the blue color emission peaking at 424 nm owing to the trivalent Ce^{3+} sensitizer, and an increase of the red color-emission peaking at 605 nm, on account of Mn^{2+} co-dopant ions, which reaches a maximum value for y = 0.4. A further enhancement of Mn^{2+} concentration (*i.e.*, $y > 0.4$) produces a decrease in the photoluminescence intensity of the red color emission because of concentration quenching.

The gap between the band of blue color-emission peaking at 424 nm due to the trivalent Ce^{3+} sensitizer and the band of red color-emission peaking at 605 nm due to the Mn^{2+} activator in the host of BLSO results in a poor color quality with low CRI values. Accordingly, a green color-emitting Tb^{3+} activator was introduced in the BLSO:Ce^{3+}/Mn^{2+} co-doped phosphors to produce high-quality white-light emission. The PL spectrum of the optimized triply-doped $Ba_{8.63}Ce_{0.09}Mn_{0.2}Tb_{0.08}Lu_2Si_6O_{24}$ phosphor under 345 nm UV light excitation is shown in Fig. 12b. The luminescence emission color of this tri-activated phosphor appears white when it is examined with the naked eye. The aforementioned experimental results show that the white-light emission that appears can be efficiently tuned from the blue to green and to the red spectral region simply by appropriately adjusting the concentration of the activated ions of the divalent Mn^{2+} and the trivalent Tb^{3+} in the BLSO host phosphor with a fixed value of the trivalent Ce^{3+} concentration.

Indeed, the CIE color coordinates of the BLSO:0.09Ce^{3+}/yMn^{2+} and BLSO:0.09Ce^{3+}/zTb^{3+} co-doped phosphors under UV light excitation at 345 nm (Fig. 12c) efficiently move from the blue color region (0.180, 0.119) to the orange-red color region (0.243, 0.328) and to the green color region (0.436, 0.243) upon increasing the values of y and z. Additionally, the CIE color coordinates of the Ce^{3+}/Mn^{2+}/Tb^{3+} tri-activated BLSO phosphors can efficiently shift towards the white-light region (0.317, 0.275); this indicates that the concentrations of the divalent Mn^{2+} and trivalent Tb^{3+} activators have appropriately been selected. For instance, at the concentration y = 0.2, the CIE color coordinates of the optimized BLSO:0.09Ce^{3+},0.2Mn^{2+},zTb^{3+} phosphors effectively move from the blue color region to the white light region with the enhancement of the green color component (the middle curve of Tb^{3+}, Mn^{2+} in Fig. 12c). These experimental results show that the developed BLSO:Ce^{3+}/Mn^{2+}/Tb^{3+} phosphors demonstrate tunable luminescence characteristics and, therefore, have superior potential as candidates for use in single PC-WLEDs. In order to shed light on the efficient tuning of the light emitting color in the entire visible region, a schematic representation of the energy transfer is shown in Fig. 12d. According to this scheme, the excitation at 345 nm effectively excites the trivalent Ce^{3+} activator. Then, through a radiative process, some Ce^{3+} dopant ions return to their ground states of $^2F_{7/2}$ or $^2F_{5/2}$, while other excited Ce^{3+} ions transfer their energy to the $^5D_2$/$^5D_3$ state of Tb^{3+} and to the $^4A_1$(4G) state of Mn^{2+}.

The high value of CRI and the stability of the light performance against the temperature of phosphors are of crucial importance in white LED applications. The influence of temperature on the emission intensity of the produced BLSO:0.09Ce^{3+}/0.2Mn^{2+}/0.08Tb^{3+} optimized phosphor was recorded over the wide temperature range of 25–200 °C, where a white LED normally works

(Fig. 12e). The increase of temperature causes a decrease in intensity of the photoluminescence emission and the remaining intensity of the tri-activated BLSO phosphor is 77% of that at room temperature when the temperature increases to 150 °C.

4.2.2 Ce^{3+}–Eu^{2+}–Mn^{2+}. As has already been discussed, Eu^{2+}, Ce^{3+}, and Mn^{2+} emit characteristic blue, green, and red colors in singly and co-doped BLSO phosphors. C. Zhang[106] and co-workers synthesized tunable full-color emitting (410–750 nm) single-phase BLSO phosphors by a high-temperature solid-state reaction method. The red emission of the divalent Mn^{2+} was effectively enhanced through an efficient energy transfer from both Ce^{3+} and Eu^{2+} activators. The present paper reports on BLSO:Eu^{2+}/Ce^{3+}/Mn^{2+} single-phase phosphors as potential candidates for near-UV-based white LEDs.

In order to shed light on the efficient energy transfer and the generation of white light by single-phase Eu^{2+}/Ce^{3+}/Mn^{2+} tri-activated BLSO phosphors, the room temperature PLE and PL spectra of the BLSO:5%Eu^{2+}, BLSO:10%Ce^{3+}, and BLSO:10%Mn^{2+} singly-doped phosphors were recorded (Fig. 13a). It is observed that the excitation spectrum of the BLSO:10%Mn^{2+} overlaps with both the emission spectra of BLSO:5%Eu^{2+} and BLSO:10%Ce^{3+}. This suggests the possibility of energy transfer from both the Eu^{2+} and Ce^{3+} to Mn^{2+} activators.

The concentrations of Eu^{2+} and Mn^{2+} were optimized as $x = 0.01$ and $z = 0.15$. Then, the concentration of Ce^{3+} was suitably adjusted to generate efficient white light. The PL spectra of the BLSO:1%Eu^{2+}/$y$$Ce^{3+}$/15%$Mn^{2+}$ (y = 0.05–0.30) are presented in Fig. 13b. Both the green and the red emission, attributed to Ce^{3+} and Mn^{2+} ions, respectively, are improved when $y > 0.1$. Consequently, deficient green-color emission is obtained in the BLSO:1%Eu^{2+} and 15%Mn^{2+} co-doped phosphors, but the red-color emission of Mn^{2+} is enhanced by efficient energy transfer from Ce^{3+} to Mn^{2+} in the BLSO:1%Eu^{2+}/30%Ce^{3+}/15%Mn^{2+} tri-activated phosphor.

The CIE chromaticity coordinate diagram of the BLSO:1%Eu^{2+}/$y$$Ce^{3+}$/15%$Mn^{2+}$ tri-activated phosphors is shown in Fig. 13c. The photoluminescence emission color is efficiently tuned to the white-light region and the CIE coordinates are tuned from (0.284, 0.228) to (0.314, 0.375) upon increasing the Ce^{3+} concentration from y = 0.05 to 0.30, respectively.

The temperature stability of the white-color emission of the single-phase BLSO phosphors was measured in the temperature range of 25–300 °C (Fig. 13d). The luminescence intensity is strongly influenced by the temperature increase and only 58% of the initial luminescence intensity at room temperature (RT) remains at 160 °C. Nonetheless, the CRI and CCT values, shown in the insets of Fig. 13d, remain unchanged with increasing temperature, indicating good color stability for BLSO phosphors.

Finally, a white LED was fabricated by coating a 395 nm UV emitting chip with the optimized single-phase white-light-emitting Eu^{2+}/Ce^{3+}/Mn^{2+} tri-activated BLSO phosphor. The electroluminescence emission spectrum of the fabricated device is shown in Fig. 13e. High-quality white light, with a 6300 K CCT value and a high CRI of 85% due to full-color emission, was produced (inset of Fig. 13e). These results indicate the excellent performance of the Eu^{2+}/Ce^{3+}/Mn^{2+} tri-activated BLSO single-phase phosphors in near-UV-based LEDs.

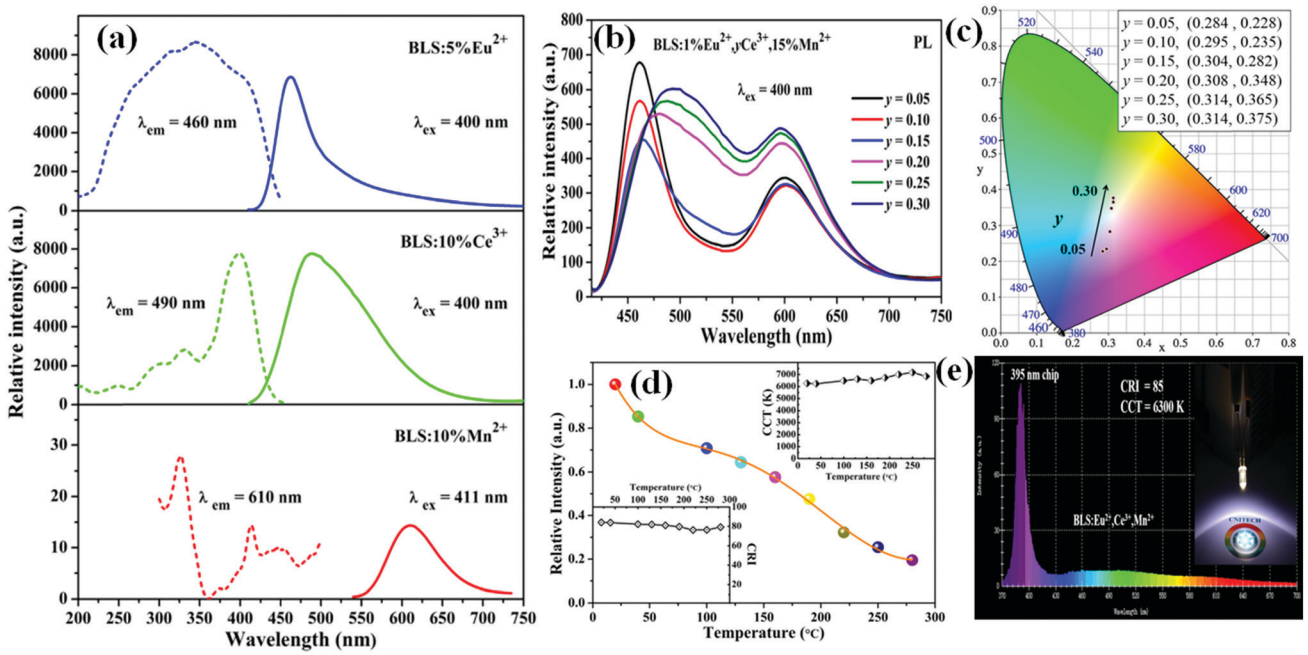

Fig. 13 (a) PLE and PL spectra of singly-doped BLSO phosphors with 5%Eu^{2+}, 10%Ce^{3+} and 10%Mn^{2+}, (b) PL spectra of BLSO:1%Eu^{2+}/$y$$Ce^{3+}$/15%$Mn^{2+}$ (y = 0.05–0.30) phosphors under 400 nm excitation, (c) CIE chromaticity coordinate diagram of BLSO:1%Eu^{2+}/$y$$Ce^{3+}$/15%$Mn^{2+}$ phosphors (y = 0.05–0.30), (d) temperature dependence of the PL spectrum and the corresponding CRI and CCT in the insets, and (e) electroluminescence emission spectrum of the fabricated LED along with its digital photograph.[106] (Reproduced with permission from ref. 106, copyright 2016 Elsevier.)

5. Other potential applications of BLSO phosphors

Apart from the aforementioned applications, the excellent photoluminescence properties and the tuning ability of BLSO phosphors also qualify them for further consideration and experimentation as well as potential use in several other emerging technologies.

For instance, F. Chi[135] and co-workers recently used Zn_2GeO_4:Mn^{2+} phosphors as multimodal temperature-sensing devices in a highly sensitive luminescence thermometer. As discussed in the earlier section (Section 2.1), Eu^{2+}-doped BLSO phosphors show red emission at low temperatures. More interestingly, changes appear in the photoluminescence emission peaks of the Eu^{2+}-activated BLSO phosphors at various temperatures. Hence, a potential application as a low-temperature optical thermometer is proposed.

Reversible photoluminescence switching based on photochromism has also attracted great attention owing to widespread potential application in anti-counterfeiting, photoswitching, and optical information storage. Y. Lv[136] and co-workers successfully used $Sr_6Ca_4(PO_4)_6F_2$:Eu^{2+} phosphors as reversible photoluminescence switching materials. The BLSO phosphors also provide various crystallographic sites for occupation by various activators. Efficient energy transfer among single activators doped in various crystallographic sites and in various activators was also observed in these phosphors. Accordingly, BLSO phosphors reveal their potential for use in reversible photoluminescence switching applications.

A different aspect was presented by L. Dai[137] and co-workers, who investigated the influence of various compositions, as a flux, on the luminescence spectra of BLSO phosphors. More specifically, they demonstrated efficient color tuning by the addition of Li_2CO_3 as a flux in BLSO phosphors. This study also demonstrates the high potential of BLSO phosphors, within a range of various compositions, for application in various color-emission and detection systems.

6. Concluding remarks

Phosphors with a general chemical composition of $Ba_9Lu_2Si_6O_{24}$ (BLSO) constitute an important part of the family of inorganic materials, where multiple cation substitutions can be made to develop optimized compositions for use in the different fields of lighting. Through this review, the concepts of (a) crystal-site engineering, in order to achieve efficient tuning of color emission, and (b) the increase and the tunability of sensitizer emission, as a result of the efficient energy-transfer phenomenon, *via* doping with different rare-earth (RE) and transition metal (TM) ions, such as Eu^{2+}, Ce^{3+}, Bi^{3+}, and Mn^{2+}, emerged.

In the light of this general consideration, the review ultimately aims at highlighting the future aspects as far as the substitution of various elements for Ba^{2+} and Lu^{3+} cations is concerned. More specifically:

(1) Broadband yellow emitting YAG:Ce^{3+} phosphors are the most commonly used and commercial materials for single-phase phosphor converted white-LEDs. The unique broadband emission of Ce^{3+} results from the strong crystal field splitting of the 5d level of the trivalent Ce^{3+} activators. Furthermore, it is noted that the temperature quenching of the Ce^{3+} doped YAG phosphors is attributed to the higher concentration of activators. The capacity of accommodating a higher concentration of the doped activators in multiple crystallographic sites of single-phase phosphors not only tunes the photoluminescence excitation and emission but also efficiently enhances the thermal stability of phosphors. Therefore, the application of phosphors with multiple crystallographic sites in high-power white LEDs is also possible.

New broadband white-light-emitting phosphors are still highly required to replace traditional YAG:Ce^{3+} phosphors. Crystal site engineering with substitution of various cations and anions would enlarge the family of single-phase phosphor converted white LEDs. The first general aspect in the model of BLSO phosphors deals with the enhancement of the higher-wavelength emission peak in the yellow to red spectral region through various substitutions of cationic and anionic ions *via* the approach of crystal-site engineering. Until recently, the substitution with only smaller ionic radii elements has been reported, which leads to contraction of the host lattice. Nevertheless, the expansion of the host lattice also leads to an efficient tuning of the photoluminescence characteristics. Thus, substitution with cations with bigger ionic radii is proposed for Ba^{2+} and Lu^{2+} in BLSO phosphors for future development. Furthermore, substitution with anions such as S^{2-}, N^{3-}, and C^{4-} is also an efficient possibility of luminescence tuning and stability enhancement. This research requires a strong background of theoretical and experimental knowledge of the various features of the inorganic materials involved.

(2) The packing of commercially available YAG:Ce^{3+} phosphors in phosphor-converted LEDs is another considerable issue to extract emission light, which attracts both scientific and technological attention. Various factors such as the particle size of phosphors along with dispersion and the microstructure of available packages are the important parameters that play effective roles in the performance in terms of light extraction efficiency of phosphor-converted LEDs. Therefore, the second aspect of this work is associated with the enormous challenge of the development of novel single-phase phosphors with high luminescence stability, an appropriate spectrum of absorption, excitation, and emission bands in the desired visible spectral region with high photoluminescence quantum efficiency, along with efficiently high color purity over a broad temperature range of 25–150 °C.

Motivation for the development of high-performance single-phase phosphors is driven to exploit the possibility of low-cost high quality warm white light generation. The surrounding environment of the host lattice around the doped activators (Eu^{2+}/Ce^{3+}) is the most essential component in the performance of phosphors for white LEDs. Therefore, the computational

design of phosphors could be first considered for selecting an appropriate host lattice for the doping with a specific activator. More specifically, the energy level of the specific activator in the design of coordination environments could be first calculated by using various simulation approaches. After optimization with various simulation approaches the target phosphors should be experimentally synthesized.

(3) Another approach for the generation of efficient white light is the combination of various color emitting phosphors (RGB phosphors) with a near-UV emitting chip. However, there is also some big challenging issues in both the chips and phosphors combination. More specifically, the near-UV emitting chip suffers from lower efficiency, which leads to the development of white LEDs with lower luminous efficacy. The combination of various color-emitting phosphors also results in degraded performance (*i.e.*, lower luminous efficiency and shorter operational lifetimes) due to the reabsorption phenomenon. More specifically, it is rare to find red-emitting phosphors that absorb only near-UV light and do not absorb any visible light. Most of the popular red-emitting phosphors are nitrides and oxynitrides doped with Eu^{2+}/Ce^{3+} and Yb^{3+} activators respectively. However, these phosphors not only absorb near-UV light but would also absorb some portion of the blue and green spectral regions.

Furthermore, the development of near-UV pumped phosphor converted LED devices implies the combination of different multiple-color-emitting phosphors. Therefore, it is beyond any doubt that this inevitable complexity of the devices plausibly enhances the cost of the fabricated white-LED devices. Moreover, the currently available single-phase full-color white light-emitting materials have the superiority of easy fabrication. However, they exhibit weak absorption with low-energy transfer efficiency and show lower performance with balancing of the high color rendering index (CRI) and lower correlated color temperature. Both these factors, *i.e.* device-development complications entailing the subsequent increase in cost and the importance of luminescence efficiency, are serious issues that have to be addressed, perhaps *via* the development of single-phase phosphors doped with single activators in order to generate full-color emission in the visible light region.

(4) Although several types of phosphor converted white-LEDs are commercialized for general illumination, there is still more room for advancement in the production of broadband single-phase white-light-emitting phosphors to increase lumen performance and cost competitiveness. The photoluminescence behavior of phosphors is one of the most important factors in enhancing the luminescence efficiency, and the coating of single-phase phosphors is an easy and low-cost method for the generation of white LEDs. A variety of novel functional materials and concepts are still in the research stage, with the potential to produce white-light with high lumen efficiency and low cost. The development of highly efficient broadband white-light-emitting single-phase phosphors and novel LED chips will efficiently trigger each other's development in the near future.

Conflicts of interest

There are no conflicts to declare.

Acknowledgements

This work was financially supported by a grant from the National Natural Science Foundation of China, U1830116, U2130112, and 62175205, the Natural Science Foundation of Fujian Province (2020J06009), the NSAF (grant no. U1830116), the Open Fund of State Key Laboratory of Applied Optics (SKLAO2020001A15), the Fundamental Research Funds for the Central Universities (Grant No. 20720190010) and Xiamen Science and Technology Bureau (3502Z20203006). The authors extend their sincere appreciation to the Deanship of Scientific Research at King Saud University, Riyadh, Saudi Arabia for funding this research group (RG-1439-087).

References

1 R. Li, J. Zhang, Z. Qiu, J. Han, J. Zhang, W. Zhou, L. Yu and S. Lian, Multiple Spectral Tunability in Single Eu 2+ -Doped (Ba, Sr) 5 (PO 4) 3 Br Phosphor, *Inorg. Chem. Front.*, 2020, **7**, 2515–2522.

2 Z. Qiu, W. Zhou, Z. Ma, J. Zhang, S. Lian and R.-S. Liu, An insight into the preferential substitution and structure repair in Eu 2+-doped whitlockite-type phosphors based on the combined experimental and theoretical calculations, *J. Mater. Chem. C*, 2019, **7**(29), 8954–8961.

3 H. Yan, Z. Qiu, J. Zhang, L. Yu, S. Lian, Z. Ma and W. Zhou, Cation vacancy repair towards a new yellow Ca7Sr3Na (PO4) 7: Eu2+ phosphor, *Ceram. Int.*, 2019, **45**(14), 16963–16968.

4 Y. Li, Z. Qiu, J. Zhang, X. Ji, X. Zhang, S. Liao, W. Zhou, L. Yu and S. Lian, Highly efficient and thermally stable single-activator white-emitting phosphor K2Ca(PO 4) F: Eu 2+ for white light-emitting diodes, *J. Mater. Chem. C*, 2019, **7**(29), 8982–8991.

5 J. Zhang, T. Zhang, Z. Qiu, S. Liu, J. Zhang, W. Zhou, L. Yu and S. Lian, Fine-Tunable self-activated luminescence in apatite-type (Ba, Sr) 5 (PO4) 3Br and the defect process, *Inorg. Chem.*, 2018, **57**(19), 12354–12363.

6 J. Luo, X. Wang, S. Li, J. Liu, Y. Guo, G. Niu, L. Yao, Y. Fu, L. Gao and Q. Dong, Efficient and stable emission of warm-white light from lead-free halide double perovskites, *Nature*, 2018, **563**(7732), 541–545.

7 P. Shen, T. Vogt and Y. Lee, Pressure Induced Enhancement of Broadband White Light Emission in Butylammonium Lead Bromide, *J. Phys. Chem. Lett.*, 2020, **11**, 4131–4137.

8 S. A. Khan, C. Li, A. Jalil, X. Xin, J. Zhu and S. Agathopoulos, Development of Structure and Tuning Ability of the Luminescence of Lead-Free Halide Perovskite Nanocrystals (NCs), *Chem. Eng. J.*, 2020, 127603.

9 M. Cui, J. Wang, M. Shang, J. Li, Q. Wei, P. Dang, H. S. Jang and J. Lin, Full visible light emission in Eu^{2+}, Mn^{2+}-doped

Ca_9 $LiY_{0.667}$ $(PO_4)_7$ phosphors based on multiple crystal lattice substitution and energy transfer for warm white LEDs with high colour-rendering, *J. Mater. Chem. C*, 2019, **7**(12), 3644–3655.

10 M. Chen, Z. Xia, M. S. Molokeev, C. C. Lin, C. Su, Y.-C. Chuang and Q. Liu, Probing Eu^{2+} luminescence from different crystallographic sites in $Ca_{10}M$ $(PO_4)_7$: Eu^{2+} (M= Li, Na, and K) with β-Ca3 (PO4) 2-type structure, *Chem. Mater.*, 2017, **29**(17), 7563–7570.

11 X. Ji, J. Zhang, Y. Li, S. Liao, X. Zhang, Z. Yang, Z. Wang, Z. Qiu, W. Zhou and L. Yu, Improving Quantum Efficiency and Thermal Stability in Blue-Emitting Ba_{2-x} Sr_x SiO_4: Ce^{3+} Phosphor *via* Solid Solution, *Chem. Mater.*, 2018, **30**(15), 5137–5147.

12 G. Blasse and B. Grabmaier, X-ray phosphors and scintillators (counting techniques), *Luminescent Materials*, Springer, 1994, pp. 170–194.

13 B. Henderson and G. F. Imbusch, *Optical spectroscopy of inorganic solids*, Oxford University Press, 2006, vol. 44.

14 S. A. Khan, N. Z. Khan, Z. Hao, W. W. Ji, H. Abadikhah, L. Hao, X. Xu and S. Agathopoulos, Influence of substitution of Al-O for Si-N on improvement of photoluminescence properties and thermal stability of Ba2Si5N8: Eu2+ red emitting phosphors, *J. Alloys Compd.*, 2018, **730**, 249–254.

15 P. Dorenbos, Energy of the first 4f7→ 4f65d transition of Eu2+ in inorganic compounds, *J. Lumin.*, 2003, **104**(4), 239–260.

16 P. Dorenbos, Ce3+ 5d-centroid shift and vacuum referred 4f-electron binding energies of all lanthanide impurities in 150 different compounds, *J. Lumin.*, 2013, **135**, 93–104.

17 J. Han, F. Pan, M. S. Molokeev, J. Dai, M. Peng, W. Zhou and J. Wang, Redefinition of crystal structure and Bi3+ yellow luminescence with strong near-ultraviolet excitation in La3BWO9: Bi3+ phosphor for white light-emitting diodes, *ACS Appl. Mater. Interfaces*, 2018, **10**(16), 13660–13668.

18 A. Meijerink, Spectroscopy and vibronic transitions of divalent europium in $LiBaF_3$, *J. Lumin.*, 1993, **55**(3), 125–138.

19 H. A. Höppe, H. Lutz, P. Morys, W. Schnick and A. Seilmeier, Luminescence in Eu2+-doped Ba2Si5N8: fluorescence, thermoluminescence, and upconversion, *J. Phys. Chem. Solids*, 2000, **61**(12), 2001–2006.

20 C. Poesl and W. Schnick, Crystal structure and nontypical deep-red luminescence of Ca3Mg [Li2Si2N6]: Eu2+, *Chem. Mater.*, 2017, **29**(8), 3778–3784.

21 J. Zhao, Y. Liang, L. Guan, G. Wang, J. Ma, G. Dong, F. Wang, D. Wang and X. Li, From blue to cyan emission: Ce3+ and Tb3+ co-doped silicon phosphate phosphors with high thermal stability, *Phys. Chem. Chem. Phys.*, 2020, **22**(17), 9405–9414.

22 N. Yang, J. Li, Z. Zhang, D. Wen, Q. Liang, J. Zhou, J. Yan and J. Shi, A Delayed Concentration Quenching of Luminescence Caused by Eu3+-Induced Phase Transition in LaSc3 (BO3)4, *Chem. Mater.*, 2020, **32**, 6958–6967.

23 S. Wang, Y. Xu, T. Chen, W. Jiang, J. Liu, X. Zhang, W. Jiang and L. Wang, A red phosphor LaSc3 (BO3) 4: Eu3+ with zero-thermal-quenching and high quantum efficiency for LEDs, *Chem. Eng. J.*, 2020, **404**, 125912.

24 Z. Xia, C. Ma, M. S. Molokeev, Q. Liu, K. Rickert and K. R. Poeppelmeier, Chemical unit cosubstitution and tuning of photoluminescence in the Ca2 (Al1–x Mg x)(Al1–x Si1+ x) O7: Eu2+ phosphor, *J. Am. Chem. Soc.*, 2015, **137**(39), 12494–12497.

25 F. Pan, M. Zhou, J. Zhang, X. Zhang, J. Wang, L. Huang, X. Kuang and M. Wu, Double substitution induced tunable luminescent properties of Ca 3−x Y x Sc 2− x Mg x Si 3 O 12: Ce 3+ phosphors for white LEDs, *J. Mater. Chem. C*, 2016, **4**(24), 5671–5678.

26 Z. Xia, G. Liu, J. Wen, Z. Mei, M. Balasubramanian, M. S. Molokeev, L. Peng, L. Gu, D. J. Miller and Q. Liu, Tuning of Photoluminescence by Cation Nanosegregation in the (CaMg) x (NaSc) 1–x Si2O6 Solid Solution, *J. Am. Chem. Soc.*, 2016, **138**(4), 1158–1161.

27 P. Dorenbos, J. Andriessen and C. Van Eijk, 4fn− 15d centroid shift in lanthanides and relation with anion polarizability, covalency, and cation electronegativity, *J. Solid State Chem.*, 2003, **171**(1-2), 133–136.

28 J. Han, W. Zhou, Z. Qiu, L. Yu, J. Zhang, Q. Xie, J. Wang and S. Lian, Redistribution of activator tuning of photoluminescence by isovalent and aliovalent cation substitutions in whitlockite phosphors, *J. Phys. Chem. C*, 2015, **119**(29), 16853–16859.

29 J. L. Wu, G. Gundiah and A. Cheetham, Structure–property correlations in Ce-doped garnet phosphors for use in solid state lighting, *Chem. Phys. Lett.*, 2007, **441**(4-6), 250–254.

30 P. Dorenbos, Crystal field splitting of lanthanide 4fn− 15d-levels in inorganic compounds, *J. Alloys Compd.*, 2002, **341**(1–2), 156–159.

31 A. Kalaji, M. Mikami and A. K. Cheetham, Ce3+-activated γ-Ca2SiO4 and other olivine-type ABXO4 phosphors for solid-state lighting, *Chem. Mater.*, 2014, **26**(13), 3966–3975.

32 M. Shang, J. Fan, H. Lian, Y. Zhang, D. Geng and J. Lin, A double substitution of Mg2+ –Si4+/Ge4+ for Al (1) 3+ –Al (2) 3+ in Ce3+ -doped garnet phosphor for white LEDs, *Inorg. Chem.*, 2014, **53**(14), 7748–7755.

33 S. A. Khan, Z. Hao, W. W. Ji, N. Z. Khan, H. Abadikhah, L. Hao, X. Xu, S. Agathopoulos and Q. Bao, Crystal-site engineering for developing tunable green light emitting Ba9Lu2Si6O24: Eu2+ phosphors for efficient white LEDs, *J. Alloys Compd.*, 2018, **767**, 374–381.

34 W.-T. Chen, H.-S. Sheu, R.-S. Liu and J. P. Attfield, Cation-size-mismatch tuning of photoluminescence in oxynitride phosphors, *J. Am. Chem. Soc.*, 2012, **134**(19), 8022–8025.

35 W. Y. Huang, F. Yoshimura, K. Ueda, Y. Shimomura, H. S. Sheu, T. S. Chan, H. F. Greer, W. Zhou, S. F. Hu and R. S. Liu, Nanosegregation and Neighbor-Cation Control of Photoluminescence in Carbidonitridosilicate Phosphors, *Angew. Chem.*, 2013, **125**(31), 8260–8264.

36 S.-S. Wang, W.-T. Chen, Y. Li, J. Wang, H.-S. Sheu and R.-S. Liu, Neighboring-cation substitution tuning of photoluminescence by remote-controlled activator in phosphor lattice, *J. Am. Chem. Soc.*, 2013, **135**(34), 12504–12507.

37 Z. Wang, Z. Xia, M. S. Molokeev, V. V. Atuchin and Q. Liu, Blue-shift of Eu 2+ emission in (Ba, Sr) 3 Lu (PO 4) 3: Eu 2+ eulytite solid-solution phosphors resulting from release of neighbouring-cation-induced stress, *Dalton Trans.*, 2014, **43**(44), 16800–16804.

38 S. A. Khan, H. Zhong, W. Ji, L.-Y. Hao, H. Abadikhah, X. Xu, N. Z. Khan and S. Agathopoulos, Single-Phase White Light-Emitting Ca x Ba (9–x) Lu2Si6O24: Eu2+/Mn2+ Phosphors, *ACS Omega*, 2017, **2**(9), 6270–6277.

39 J. Brgoch, C. K. Borg, K. A. Denault, S. P. DenBaars and R. Seshadri, Tuning luminescent properties through solid-solution in (Ba1− xSrx) 9Sc2Si6O24: Ce3+, Li+, *Solid State Sci.*, 2013, **18**, 149–154.

40 T. Nakano, Y. Kawakami, K. Uematsu, T. Ishigaki, K. Toda and M. Sato, Novel Ba–Sc–Si-oxide and oxynitride phosphors for white LED, *J. Lumin.*, 2009, **129**(12), 1654–1657.

41 J. Brgoch, C. K. Borg, K. A. Denault, A. Mikhailovsky, S. P. DenBaars and R. Seshadri, An efficient, thermally stable cerium-based silicate phosphor for solid state white lighting, *Inorg. Chem.*, 2013, **52**(14), 8010–8016.

42 C. Hu, B. Peng, K. X. Song, B. Liu, D. Wang and I. M. Reaney, The cyan-green luminescent behaviour of nitrided Ba9Y2Si6O24: Eu2+ phosphors for W-LED, *Ceram. Int.*, 2018, **44**, S2–S6.

43 H. Guo, Z. Zheng, L. Teng, R. Wei and F. Hu, Tunable white-light emission and energy transfer in single-phase Bi3+, Eu3+ co-doped Ba9Y2Si6O24 phosphors for UV w-LEDs, *J. Lumin.*, 2019, **213**, 494–503.

44 Z. Zhang, W. Zhou, Z. Zhang, Q. Wang and S. Li, Preparation and luminescence properties of Ba 9 Y 2 Si 6 O 24: Sm 3+ phosphors with excellent thermal stability for solid-state lightning, *Appl. Phys. A: Mater. Sci. Process.*, 2021, **127**(5), 1–8.

45 Y. J. L. Teng, Luminescence of the near-ultraviolet blue-emitting Ba9Al2Si6O24: Ce3+ phosphor, *Luminescence*, 2021, **36**(1), 256–260.

46 Y. Liu, J. Zhang, C. Zhang, J. Xu, G. Liu, J. Jiang and H. Jiang, Ba9Lu2Si6O24: Ce3+: an efficient green phosphor with high thermal and radiation stability for solid-state lighting, *Adv. Opt. Mater.*, 2015, **3**(8), 1096–1101.

47 Y. Liu, C. Zhang, Z. Cheng, Z. Zhou, J. Jiang and H. Jiang, Origin and luminescence of anomalous red-emitting center in rhombohedral Ba9Lu2Si6O24: Eu2+ blue phosphor, *Inorg. Chem.*, 2016, **55**(17), 8628–8635.

48 S. A. Khan, Z. Hao, W. W. Ji, N. Z. Khan, H. Abadikhah, L. Hao, X. Xu, S. Agathopoulos and Q. Bao, Compounds, Crystal-site engineering for developing tunable green light emitting Ba9Lu2Si6O24: Eu2+ phosphors for efficient white LEDs, *J. Alloys Compd.*, 2018, **767**, 374–381.

49 Y. Guo, S. H. Park, B. C. Choi, J. H. Jeong and J. H. Kim, Dual-Mode Manipulating Multicenter Photoluminescence in a Single-Phased Ba 9 Lu 2 Si 6 O 24: Bi 3+, Eu 3+ Phosphor to Realize White Light/Tunable Emissions, *Sci. Rep.*, 2017, **7**(1), 1–11.

50 Y. Liu, J. Zhang, C. Zhang, J. Jiang and H. J. T. Jiang, High efficiency green phosphor Ba9Lu2Si6O24: Tb3+: visible quantum cutting via cross-relaxation energy transfers, *J. Phys. Chem. C*, 2016, **120**(4), 2362–2370.

51 J. Zhou and Z. Xia, Luminescence color tuning of Ce 3+, Tb 3+ and Eu 3+ codoped and tri-doped BaY 2 Si 3 O 10 phosphors via energy transfer, *J. Mater. Chem. C*, 2015, **3**(29), 7552–7560.

52 M. Shang, C. Li and J. Lin, How to produce white light in a single-phase host?, *Chem. Soc. Rev.*, 2014, **43**(5), 1372–1386.

53 H. Jiao and Y. Wang, Ca2Al2SiO7: Ce3+, Tb3+: a white-light phosphor suitable for white-light-emitting diodes, *J. Electrochem. Soc.*, 2009, **156**(5), J117.

54 D. Jia, J. Zhu and B. Wu, Trapping centers in CaS: Bi3+ and CaS: Eu2+, Tm3+, *J. Electrochem. Soc.*, 2000, **147**(1), 386.

55 S. A. Khan, W. Ji, L. Hao, X. Xu, S. Agathopoulos and N. Z. Khan, Synthesis and characterization of Ce3+/Tb3+ co–doped CaLa4Si3O13 phosphors for application in white LED, *Opt. Mater.*, 2017, **72**, 637–643.

56 C.-H. Huang, T.-M. Chen, W.-R. Liu, Y.-C. Chiu, Y.-T. Yeh and S.-M. Jang, A single-phased emission-tunable phosphor Ca9Y (PO4) 7: Eu2+, Mn2+ with efficient energy transfer for white-light-emitting diodes, *ACS Appl. Mater. Interfaces*, 2010, **2**(1), 259–264.

57 Q. Bai, Z. Wang, P. Li, S. Xu, T. Li and Z. Yang, Tunable blue-green emitting and energy transfer of a Eu 2+/Tb 3+ codoped Sr 3 La (PO 4) 3 phosphor for near-UV white LEDs, *New J. Chem.*, 2015, **39**(11), 8933–8939.

58 M. Jiao, N. Guo, W. Lü, Y. Jia, W. Lv, Q. Zhao, B. Shao and H. You, Tunable blue-green-emitting Ba3LaNa (PO4) 3F: Eu2+, Tb3+ phosphor with energy transfer for near-UV white LEDs, *Inorg. Chem.*, 2013, **52**(18), 10340–10346.

59 H. Chen and Y. Wang, Sr2LiScB4O10: Ce3+/Tb3+: a green-emitting phosphor with high energy transfer efficiency and stability for LEDs and FEDs, *Inorg. Chem.*, 2019, **58**(11), 7440–7452.

60 S. A. Khan, N. Z. Khan, W. W. Ji, L. Ali, H. Abadikhah, L. Hao, X. Xu, S. Agathopoulos, Q. Khan and L. Zhu, Luminescence properties and energy transfer in Ce3+/Tb3+ co–doped Y5Si3O12N oxynitride phosphors, *Dyes Pigm.*, 2019, **160**, 675–682.

61 S. A. Khan, Z. Hao, H. Wei-Wei, L.-Y. Hao, X. Xu, N. Z. Khan and S. Agathopoulos, Novel single-phase full-color emitting Ba 9 Lu 2 Si 6 O 24: Ce 3+/Mn 2+/Tb 3+ phosphors for white LED applications, *J. Mater. Sci.*, 2017, **52**(18), 10927–10937.

62 S. A. Khan, A. Jalil, Q. U. Khan, R. M. Irfan, I. Mehmood, K. Khan, M. Kiani, B. Dong, N. Z. Khan and J.-L. Yu, New physical insight into crystal structure, luminescence and optical properties of YPO4: Dy3+/Eu3+/Tb3+ single-phase white-light-emitting phosphors, *J. Alloys Compd.*, 2020, **817**, 152687.

63 N. Z. Khan, S. A. Khan, L. Zhan, A. Jalil, J. Ahmed, M. M. Khan, M. T. Abbas, F. Wang and X. Xu, Synthesis, structure and photoluminescence properties of Ca2YTaO6: Bi3+ /Eu3+ double perovskite white light emitting phosphors, *J. Alloys Compd.*, 2021, **868**, 159257.

64 N. Z. Khan, S. A. Khan, M. Sohail, M. M. Khan, J. Ahmed, L. Zhan, F. Wang, M. T. Abbas and X. Xu, Single Phase Multi Color Emitting Ca_2LuTaO_6: Dy3+/Eu3+ Double Perovskite Oxide Phosphors, *J. Am. Ceram. Soc.*, 2021, **104**, 4911–4922.

65 S. A. Khan, N. Z. Khan, I. Mehmood, M. Rauf, B. Dong, M. Kiani, J. Ahmed, S. M. Alshehri, J. Zhu and S. Agathopoulos, Broad band white-light-emitting Y5Si3O12N: Ce3+/Dy3+ oxonitridosilicate phosphors for solid state lighting applications, *J. Lumin.*, 2021, **229**, 117687.

66 Y. Liu, J. Zhang, C. Zhang, J. Xu, G. Liu, J. Jiang and H. Jiang, Ba9Lu2Si6O24: Ce3+: an efficient green phosphor with high thermal and radiation stability for solid-state lighting, *Adv. Opt. Mater.*, 2015, **3**(8), 1096–1101.

67 R. Deng, F. Qin, R. Chen, W. Huang, M. Hong and X. Liu, Temporal full-colour tuning through non-steady-state upconversion, *Nat. Nanotechnol.*, 2015, **10**(3), 237–242.

68 N. Pradhan, D. Goorskey, J. Thessing and X. Peng, An alternative of CdSe nanocrystal emitters: pure and tunable impurity emissions in ZnSe nanocrystals, *J. Am. Chem. Soc.*, 2005, **127**(50), 17586–17587.

69 J. B. Pollock, G. L. Schneider, T. R. Cook, A. S. Davies and P. J. Stang, Tunable visible light emission of self-assembled rhomboidal metallacycles, *J. Am. Chem. Soc.*, 2013, **135**(37), 13676–13679.

70 I. L. Medintz, H. T. Uyeda, E. R. Goldman and H. Mattoussi, Quantum dot bioconjugates for imaging, labelling and sensing, *Nat. Mater.*, 2005, **4**(6), 435–446.

71 T. Kuykendall, P. Ulrich, S. Aloni and P. Yang, Complete composition tunability of InGaN nanowires using a combinatorial approach, *Nat. Mater.*, 2007, **6**(12), 951–956.

72 S. Gai, C. Li, P. Yang and J. Lin, Recent progress in rare earth micro/nanocrystals: soft chemical synthesis, luminescent properties, and biomedical applications, *Chem. Rev.*, 2014, **114**(4), 2343–2389.

73 S. Zhou, N. Jiang, B. Wu, J. Hao and J. Qiu, Ligand-driven wavelength-tunable and ultra-broadband infrared luminescence in single-ion-doped transparent hybrid materials, *Adv. Funct. Mater.*, 2009, **19**(13), 2081–2088.

74 W. B. Park, S. P. Singh, C. Yoon and K.-S. Sohn, Eu 2+ luminescence from 5 different crystallographic sites in a novel red phosphor, Ca 15 Si 20 O 10 N 30: Eu 2+, *J. Mater. Chem.*, 2012, **22**(28), 14068–14075.

75 Y.-T. Tsai, C.-Y. Chiang, W. Zhou, J.-F. Lee, H.-S. Sheu and R.-S. Liu, Structural ordering and charge variation induced by cation substitution in (Sr, Ca) AlSiN3: Eu phosphor, *J. Am. Chem. Soc.*, 2015, **137**(28), 8936–8939.

76 K. A. Denault, J. Brgoch, M. W. Gaultois, A. Mikhailovsky, R. Petry, H. Winkler, S. P. DenBaars and R. Seshadri, Consequences of optimal bond valence on structural rigidity and improved luminescence properties in Sr x Ba2–x SiO4: Eu2+ orthosilicate phosphors, *Chem. Mater.*, 2014, **26**(7), 2275–2282.

77 Y. Sato, H. Kato, M. Kobayashi, T. Masaki, D. H. Yoon and M. Kakihana, Tailoring of deep-red luminescence in Ca2SiO4: Eu2+, *Angew. Chem., Int. Ed.*, 2014, **53**(30), 7756–7759.

78 Z. Zhao, Z. Yang, Y. Shi, C. Wang, B. Liu, G. Zhu and Y. Wang, Red-emitting oxonitridosilicate phosphors Sr 2 SiN z O 4− 1.5 z: Eu 2+ for white light-emitting diodes: structure and luminescence properties, *J. Mater. Chem. C*, 2013, **1**(7), 1407–1412.

79 N. Komuro, M. Mikami, Y. Shimomura, E. G. Bithell and A. K. Cheetham, Synthesis, structure and optical properties of cerium-doped calcium barium phosphate–a novel blue-green phosphor for solid-state lighting, *J. Mater. Chem. C*, 2015, **3**(1), 204–210.

80 W. B. Park, S. P. Singh and K.-S. Sohn, Discovery of a phosphor for light emitting diode applications and its structural determination, Ba (Si, Al) 5 (O, N) 8: Eu2+, *J. Am. Chem. Soc.*, 2014, **136**(6), 2363–2373.

81 Y. Kawano, S. W. Kim, T. Ishigaki, K. Uematsu, K. Toda, H. Takaba and M. Sato, Site engineering concept of Ce 3+ -activated novel orange-red emission oxide phosphors, *Opt. Mater. Express*, 2014, **4**(9), 1770–1774.

82 H. Funakubo, T. Watanabe, T. Kojima, T. Sakai, Y. Noguchi, M. Miyayama, M. Osada, M. Kakihana and K. Saito, Property design of Bi4Ti3O12-based thin films using a site-engineered concept, *J. Cryst. Growth*, 2003, **248**, 180–185.

83 Y. Sato, H. Kuwahara, H. Kato, M. Kobayashi, T. Masaki and M. Kakihana, Large redshifts in emission and excitation from Eu 2+ -activated Sr 2 SiO 4 and Ba 2 SiO 4 phosphors induced by controlling Eu 2+ occupancy on the basis on crystal-site engineering, *Opt. Photonics J.*, 2015, **5**(11), 326.

84 X. Zhang, J. Wang, L. Huang, F. Pan, Y. Chen, B. Lei, M. Peng and M. Wu, Tunable luminescent properties and concentration-dependent, site-preferable distribution of Eu2+ ions in silicate glass for white LEDs applications, *ACS Appl. Mater. Interfaces*, 2015, **7**(18), 10044–10054.

85 I. Cho, G. Anoop, D. Suh, S. Lee and J. Yoo, On the stability and reliability of Sr 1-x Ba x Si 2 O 2 N 2: Eu 2+ phosphors for white LED applications, *Opt. Mater. Express*, 2012, **2**(9), 1292–1305.

86 P. Dang, G. Li, S. Liang, H. Lian and J. Lin, Multichannel photoluminescence tuning in Eu-doped apatite phosphors via coexisting cation substitution, energy transfer and valence mixing, *J. Mater. Chem. C*, 2019, **7**(20), 5975–5987.

87 S. Liu, H. Cai, S. Zhang, Z. Song, Z. Xia and Q. Liu, Site engineering strategy toward enhanced luminescence thermostability of a Cr 3+ -doped broadband NIR phosphor and its application, *Mater. Chem. Front.*, 2021, **5**(10), 3841–3849.

88 Q. Zhang, G. Li, P. Dang, D. Liu, D. Huang, H. Lian and J. Lin, Enhancing and tuning broadband near-infrared (NIR) photoluminescence properties in Cr 3+ -doped Ca 2 YHf2Al3O12 garnet phosphors via Ce 3+/Yb 3+ -codoping for LED applications, *J. Mater. Chem. C*, 2021, **9**(14), 4815–4824.

89 S. A. Khan, N. Z. Khan, I. Mehmood, M. Rauf, B. Dong, M. Kiani, J. Ahmed, S. M. Alshehri, J. Zhu and S. Agathopoulos, Broad band white-light-emitting Y5Si3O12N: Ce3+/Dy3+ oxonitridosilicate phosphors for

solid state lighting applications, *J. Lumin.*, 2021, **229**, 117687.

90 Y. Liu, C. Zhang, Z. Cheng, Z. Zhou, J. Jiang and H. Jiang, Origin and luminescence of anomalous red-emitting center in rhombohedral Ba9Lu2Si6O24: Eu2+ blue phosphor, *Inorg. Chem.*, 2016, **55**(17), 8628–8635.

91 T. Nakano, Y. Kawakami, K. Uematsu, T. Ishigaki, K. Toda and M. Sato, Novel Ba–Sc–Si-oxide and oxynitride phosphors for white LED, *J. Lumin.*, 2009, **129**(12), 1654–1657.

92 Y. Kim and S. Park, Preparation and luminescent properties of Eu-substituted barium–yttrium orthosilicate phosphors, *Opt. Mater.*, 2013, **36**(2), 458–462.

93 L. Bian, T. Zhou, J. Yang, Z. Song and Q. Liu, Crystal structure and photoluminescence of (Ba1− x− ySryEux) 9Sc2Si6O24, *J. Lumin.*, 2012, **132**(10), 2541–2545.

94 S. K. Amoah, L. P. Sandjo, J. M. Kratz and M. W. Biavatti, Rosmarinic acid–pharmaceutical and clinical aspects, *Planta Med.*, 2016, **82**(05), 388–406.

95 J. Tang, J. Chen, L. Hao, X. Xu, W. Xie and Q. Li, Green Eu2+ -doped Ba3Si6O12N2 phosphor for white light-emitting diodes: Synthesis, characterization and theoretical simulation, *J. Lumin.*, 2011, **131**(6), 1101–1106.

96 J. Brgoch, C. K. Borg, K. A. Denault, A. Mikhailovsky, S. P. DenBaars and R. Seshadri, An efficient, thermally stable cerium-based silicate phosphor for solid state white lighting, *Inorg. Chem.*, 2013, **52**(14), 8010–8016.

97 L. Bian, F. Du, S. Yang, Q. Ren and Q. Liu, Crystal structure and near-ultraviolet photoluminescence properties of Ba9Sc2Si6O24: Ce3+, Na +, *J. Lumin.*, 2013, **137**, 168–172.

98 X. Zhang, Y. Liu, J. Lin, Z. Hao, Y. Luo, Q. Liu and J. Zhang, Optical properties and energy transfers of Ce3+ and Mn2+ in Ba9Sc2 (SiO4) 6, *J. Lumin.*, 2014, **146**, 321–324.

99 P. D. Rack and P. H. Holloway, The structure, device physics, and material properties of thin film electroluminescent displays, *Mater. Sci. Eng., R*, 1998, **21**(4), 171–219.

100 R.-H. Yan, H. Ding, L. Gao, D.-Y. Chen, L.-W. Yin, A.-L. Xu, H.-L. Lv, X. Xu, L.-C. Ju and L.-J. Yin, Surface passivation of applying a thin carbon coating toward significantly thermal stable SrSi2O2N2: Eu2+ green phosphors, *Mater. Chem. Phys.*, 2020, **256**, 123759.

101 H.-R. Chen, C. Cai, Z.-W. Zhang, Y.-J. Zhao, L. Zhang, X. Wang, L.-B. Zhang, X. Xu, H. Van Bui and L.-J. Yin, Achieving an efficient La3Si8N11O4: Eu2+ phosphor via chemical reduction of nano-scale carbon film: Toward white light-emitting diodes, *J. Alloys Compd.*, 2019, **799**, 360–367.

102 Y.-X. Liu, J.-X. Hu, L.-C. Ju, C. Cai, V.-B. Hao, S.-H. Zhang, Z.-W. Zhang, X. Xu, X. Jian and L.-J. Yin, Hydrophobic surface modification toward highly stable K2SiF6: Mn4+ phosphor for white light-emitting diodes, *Ceram. Int.*, 2020, **46**(7), 8811–8818.

103 R.-J. Xie, Y. Q. Li, N. Hirosaki and H. Yamamoto, *Nitride phosphors and solid-state lighting*, CRC Press, 2016.

104 C. Zhang, Y. Liu, J. Zhang, X. Zhang, J. Zhang, Z. Cheng, J. Jiang and H. Jiang, A single-phase Ba9Lu2Si6O24: Eu2+, Ce3+, Mn2+ phosphor with tunable full-color emission for NUV-based white LED applications, *Mater. Res. Bull.*, 2016, **80**, 288–294.

105 Y. Liu, J. Silver, R.-J. Xie, J. Zhang, H. Xu, H. Shao, J. Jiang and H. Jiang, An excellent cyan-emitting orthosilicate phosphor for NUV-pumped white LED application, *J. Mater. Chem. C*, 2017, **5**(47), 12365–12377.

106 C. Zhang, Y. Liu, J. Zhang, X. Zhang, J. Zhang, Z. Cheng, J. Jiang and H. Jiang, A single-phase Ba9Lu2Si6O24: Eu2+, Ce3+, Mn2+ phosphor with tunable full-color emission for NUV-based white LED applications, *Mater. Res. Bull.*, 2016, **80**, 288–294.

107 J. Brgoch, C. K. Borg, K. A. Denault, S. P. DenBaars and R. Seshadri, Tuning luminescent properties through solid-solution in (Ba1− xSrx) 9Sc2Si6O24: Ce3+, Li+, *Solid State Sci.*, 2013, **18**, 149–154.

108 F. Kang, M. Peng, S. Xu, Z. Ma, G. Dong and J. Qiu, Broadly tunable emission from CaMoO4: Bi phosphor based on locally modifying the microenvironment around Bi3+ ions, *Eur. J. Inorg. Chem.*, 2014, (8), 1373–1380.

109 F. Kang, M. Peng, Q. Zhang and J. Qiu, Abnormal anti-quenching and controllable multi-transitions of Bi3+ luminescence by temperature in a yellow-emitting LuVO4: Bi3+ phosphor for UV-converted white LEDs, *Chem. – Eur. J.*, 2014, **20**(36), 11522–11530.

110 Y. Guo, S. H. Park, B. C. Choi, J. H. Jeong and J. H. Kim, Dual-Mode Manipulating Multicenter Photoluminescence in a Single-Phased Ba 9 Lu 2 Si 6 O 24: Bi3+, Eu 3+ Phosphor to Realize White Light/Tunable Emissions, *Sci. Rep.*, 2017, **7**(1), 1–11.

111 K. Song, J. Zhang, Y. Liu, C. Zhang, J. Jiang, H. Jiang and H.-B. Qin, Red-emitting phosphor Ba9Lu2Si6O24: Ce3+, Mn2+ with enhanced energy transfer via self-charge compensation, *J. Phys. Chem. C*, 2015, **119**(43), 24558–24563.

112 Y. Liu, J. Zhang, C. Zhang, J. Jiang and H. Jiang, High efficiency green phosphor Ba9Lu2Si6O24: Tb3+: visible quantum cutting via cross-relaxation energy transfers, *J. Phys. Chem. C*, 2016, **120**(4), 2362–2370.

113 T.-J. Lee, L.-Y. Luo, E. W.-G. Diau, T.-M. Chen, B.-M. Cheng and C.-Y. Tung, Visible quantum cutting through down-conversion in green-emitting K 2 Gd F 5: Tb 3+ phosphors, *Appl. Phys. Lett.*, 2006, **89**(13), 131121.

114 H.-Y. Tzeng, B.-M. Cheng and T.-M. Chen, Visible quantum cutting in green–emitting BaGdF5: Tb3+ phosphors *via* downconversion, *J. Lumin.*, 2007, **122**, 917–920.

115 D. Wang and N. Kodama, Visible quantum cutting through downconversion in GdPO4: Tb3+ and Sr3Gd (PO4) 3: Tb3+, *J. Solid State Chem.*, 2009, **182**(8), 2219–2224.

116 Z. Hao, J. Zhang, X. Zhang, S. Lu and X. Wang, Blue-green-emitting phosphor CaSc2O4: Tb3+: tunable luminescence manipulated by cross-relaxation, *J. Electrochem. Soc.*, 2009, **156**(3), H193.

117 T. Chan, C. Lin, R. Liu, R.-J. Xie, N. Hirosaki and B.-M. Cheng, Photoluminescent and thermal stable properties of Tb3+ -doped Ca-α-SiAlON under VUV excitation, *J. Electrochem. Soc.*, 2009, **156**(7), J189.

118 H. Zhang, Y. Wang, Y. Tao, W. Li, D. Hu, E. Feng and X. Nie, Visible quantum cutting in Tb3+ -doped BaGdB9O16 via downconversion, *J. Electrochem. Soc.*, 2010, **157**(8), J293.

119 G. S. Raju, J. Y. Park, H. C. Jung, B. K. Moon, J. H. Jeong and J. H. Kim, Gd3+ sensitization effect on the luminescence properties of Tb3+ activated calcium gadolinium oxyapatite nanophosphors, *J. Electrochem. Soc.*, 2010, **158**(2), J20.

120 B. Han, H. Liang, Y. Huang, Y. Tao and Q. Su, Vacuum ultraviolet– visible spectroscopic properties of Tb3+ in Li (Y, Gd)(PO3) 4: tunable emission, quantum cutting, and energy transfer, *J. Phys. Chem. C*, 2010, **114**(14), 6770–6777.

121 M. Xie, Y. Tao, Y. Huang, H. Liang and Q. Su, The quantum cutting of Tb3+ in Ca6Ln2Na2 (PO4) 6F2 (Ln= Gd, La) under VUV– UV excitation: with and without Gd3+, *Inorg. Chem.*, 2010, **49**(24), 11317–11324.

122 X. Yan, G. R. Fern, R. Withnall and J. Silver, Effects of the host lattice and doping concentration on the colour of Tb 3+ cation emission in Y 2 O 2 S: Tb 3+ and Gd 2 O 2 S: Tb 3+ nanometer sized phosphor particles, *Nanoscale*, 2013, **5**(18), 8640–8646.

123 P. S. May and K. D. Sommer, Tb3+ luminescence in Tb-doped and Tb/Gd-doped CsCdBr3 crystals: 5D4→ 5D3 cross-relaxation rates in Tb3+ pairs, *J. Phys. Chem. A*, 1997, **101**(50), 9571–9577.

124 R. L. Tranquilin, L. X. Lovisa, C. R. Almeida, C. A. Paskocimas, M. S. Li, M. C. Oliveira, L. Gracia, J. Andrés, E. Longo and F. V. Motta, Understanding the white-emitting CaMoO4 Co-doped Eu3+, Tb3+, and Tm3+ phosphor through experiment and computation, *J. Phys. Chem. C*, 2019, **123**(30), 18536–18550.

125 B. Hou, M. Jia, P. Li, G. Liu, Z. Sun and Z. Fu, Multi-functional optical thermometry based on the rare-earth-ions-doped up-/down-conversion Ba2TiGe2O8: Ln (Ln= Eu3+/Er3+/Ho3+/Yb3+) Phosphors, *Inorg. Chem.*, 2019, **58**(12), 7939–7946.

126 C. Wang, Y. Jin, Y. Lv, G. Ju, D. Liu, L. Chen, Z. Li and Y. Hu, Trap distribution tailoring guided design of super-long-persistent phosphor Ba 2 SiO 4: Eu 2+, Ho 3+ and photostimulable luminescence for optical information storage, *J. Mater. Chem. C*, 2018, **6**(22), 6058–6067.

127 W. Zeng, Y. Wang, M. Zheng, R. Yang, Y. Luo, X. Yi and R. Zhang, Long-persistent phosphorescence in Eu2+ -doped calcium borate chloride for optical data storage, *J. Alloys Compd.*, 2020, **825**, 154143.

128 D. Zhang, C. Wang, Y. Liu, Q. Shi, W. Wang and Y. Zhai, Green and red photoluminescence from ZnAl2O4: Mn phosphors prepared by sol–gel method, *J. Lumin.*, 2012, **132**(6), 1529–1531.

129 X. Zhang, Z. Zhu, Z. Guo, Z. Sun and Y. Chen, A ratiometric optical thermometer with high sensitivity and superior signal discriminability based on Na3Sc2P3O12: Eu2+, Mn2+ thermochromic phosphor, *Chem. Eng. J.*, 2019, **356**, 413–422.

130 S. A. Khan, C. Li, A. Jalil, X. Xin, J. Zhu and S. Agathopoulos, Development of Structure and Tuning Ability of the Luminescence of Lead-Free Halide Perovskite Nanocrystals (NCs), *Chem. Eng. J.*, 2020, 127603.

131 A. Huang, Z. Yang, C. Yu, Z. Chai, J. Qiu and Z. Song, Tunable and white light emission of a single-phased Ba2Y (BO3) 2Cl: Bi3+, Eu3+ phosphor by energy transfer for ultraviolet converted white LEDs, *J. Phys. Chem. C*, 2017, **121**(9), 5267–5276.

132 H. Zhou, Q. Wang and Y. Jin, Temperature dependence of energy transfer in tunable white light-emitting phosphor BaY 2 Si 3 O 10: Bi 3+, Eu 3+ for near UV LEDs, *J. Mater. Chem. C*, 2015, **3**(42), 11151–11162.

133 Z. Xia and Q. Liu, Progress in discovery and structural design of color conversion phosphors for LEDs, *Prog. Mater. Sci.*, 2016, **84**, 59–117.

134 R. Gautier, X. Li, Z. Xia and F. Massuyeau, Two-step design of a single-doped white phosphor with high color rendering, *J. Am. Chem. Soc.*, 2017, **139**(4), 1436–1439.

135 F. Chi, B. Jiang, Z. Zhao, Y. Chen, X. Wei, C. Duan, M. Yin and W. Xu, Multimodal temperature sensing using Zn2GeO4: Mn2+ phosphor as highly sensitive luminescent thermometer, *Sens. Actuators, B*, 2019, **296**, 126640.

136 Y. Lv, Y. Jin, Z. Li, S. Zhang, H. Wu, G. Xiong, G. Ju, L. Chen, Z. Hu and Y. Hu, Reversible photoluminescence switching in photochromic material Sr 6 Ca 4 (PO 4) 6 F 2: Eu 2+ and the modified performance by trap engineering via Ln 3+ (Ln= La, Y, Gd, Lu) co-doping for erasable optical data storage, *J. Mater. Chem. C*, 2020, **8**, 6403–6412.

137 L. Dai, S. Huang, Y. Zhong, Z. Rang and Z. Zhou, Effects of flux on crystal structure and photoluminescence properties of the Ba9Lu2Si6O24: Ce3+ blue-green-emitting phosphor, *Mater. Res. Bull.*, 2017, **93**, 251–255.